Advances in Engineering Software 137 (2019) 102709

Contents lists available at ScienceDirect

Advances in Engineering Software

journal homepage: www.elsevier.com/locate/advengsoft

Research paper

Distance-based optimal sampling in a hypercube: Analogies to N-body systems

Miroslav Vořechovský*, Jan Mašek, Jan Eliáš

Institute of Structural Mechanics, Brno University of Technology, Veveří 331/95, Brno 602 00, Czech Republic

ARTICLE INFO

Keywords:
ϕ criterion
Audze-Eglājs
Maximin criterion
MiniMax criterion
Periodic space
Space-filling design
Uniform design
Robust design
Low-discrepancy
Design of experiments
Latin hypercube sampling
Monte carlo integration

ABSTRACT

A method is proposed for the construction of uniformly distributed point sets within a design domain using an analogy to a dynamical system of interacting particles. The possibility of viewing various distance-based optimality criteria as formulas representing the potential energy of a system of charged particles is discussed. The potential energy is employed in deriving the equations of motion of the particles. The particles are either attracted or repelled and dissipative dynamical systems can be simulated to achieve optimal and near-optimal arrangements of points. The design domain is set up as an N_{var}-dimensional unit hypercube, with N_{var} being the number of variables (factors). The number of points is equal to the number of simulations (levels). The periodicity assumption of the design domain is shown to be an elegant way to obtain *statistically uniform* coverage of the design domain.

The ϕ_p criterion, which is a generalization of the Maximin criterion, is selected in order to demonstrate its analogy with an N-body system. This criterion guarantees that the points are *spread uniformly* within the design domain. The solution to such an N-body system is presented. The obtained designs are shown to outperform the existing optimal designs in various types of applications: multidimensional numerical integration, statistical exploration of computer models, reliability analyses of engineering systems, and screenings or exploratory designs for the global optimization/minimization of functions.

1. Introduction

The problem of selecting "uniformly distributed points" in a rectangular domain is an old one that finds applications in many fields of science, mathematics and physics, engineering, biology, etc. [65]. The growing demand for the replacement of physical experiments by simulations based on sophisticated mathematical models consecutively generates a strong demand for the development of point sets with somewhat uniformly distributed points within the design domain. One of the possible applications of these sets is the estimation of multidimensional integrals using the Monte Carlo method. In such an analysis of transformations of random variables/vectors featured in statistical, sensitivity and reliability analyses of engineering systems, a set of points which are uniformly distributed with respect to probabilities is needed. Another application of uniformly distributed points is in the field of the optimization [62] (maximization or minimization of functions) or screenings [66] of computer models of physical experiments. Also, uniform designs obtained using methods from the field of Design of Experiments (DoE) for computer models are now being routinely used to build response surfaces or meta-models (surrogate models) that may be capable of replacing complex computational models, which are expensive to evaluate [37], see e.g. least squares-based polynomial chaos (PC) expansion [5,33] or least-squares support vector regression [73].

There are many types of design (i.e. a set of points selected from a design domain) that can be thought of as uniform in some sense. For example, *space-filling designs* [30], which can be loosely interpreted as designs that are representative of a design region, are widely used in computer experiments. Designs with good space-filling properties are mainly constructed when designing one-stage computer experiments.

When seeking a design suitable for building a response surface using Kriging [8], *distance-based criteria* have been found to be optimal [29] (e.g. the Maximin criterion [29], its relaxation to the ϕ_p criterion [44] and its special case, the Audze-Eglājs criterion [2], and the miniMax criterion [29] and its relaxed variant [61]).

The objective of observing the design domain "everywhere" is achieved by designs that minimize the "distance" between the distribution of observation sites and the uniform distribution. The notion of *discrepancy* captures this intuitive objective well (see [48, Chapter 2]) and discrepancy in a way expresses the *sample non-uniformity*.

* Corresponding author.
E-mail address: vorechovsky.m@vut.cz (M. Vořechovský).

https://doi.org/10.1016/j.advengsoft.2019.102709
Received 4 February 2019; Received in revised form 3 July 2019; Accepted 19 August 2019

Moreover, the Koksma-Hlawka inequality [32] says that decreasing the "discrepancy measure" of a design decreases the bound on the error of the integral estimated with a discrete sample set. Conceptually, the discrepancy of a sample design is an appropriate norm of the difference between the number of points per sub-volume and a uniform smearing of points. Various versions can be considered to evaluate discrepancy; they have received an analytical expression and can therefore be minimized, as with e.g. Modified L_2 discrepancy [14], Wrap-Around L_2 discrepancy [25] or Centered L_2 discrepancy [16,25], and other versions [74] (see also Santner et al. [65] for a review). As noted in [34], these general measures of discrepancy are unsatisfactory as soon as the number of dimensions exceeds a few units because they are too hard to compute.

The search for multivariate quadrature rules of minimal size with a specified polynomial accuracy has been the topic of many years of research. When dealing with multidimensional integration, Quasi Monte Carlo sequences (QMC), which are sometimes named *low-discrepancy sequences* or *digital nets*, have become popular alternatives and can be considered standard methods within this field. The use of low-discrepancy sequences provides a cheap alternative to algorithmic *discrepancy minimization* [48, Chapters. 3 & 4]. They have become, together with their randomized versions, the standard and benchmark for numerical integration.

Another frequent requirement placed on designs is *orthogonality*. The orthogonality of a design ensures that all specified parameters may be estimated independently of each other (estimation of main effects) and interactions can also be estimated in a straightforward way. There are various design types focused on orthogonality, such as various factorial designs in DoE, "orthogonal arrays" known from combinatorial designs, "mutually orthogonal latin squares", etc. Some authors simply tend to decrease the statistical correlations among the vectors of samples of individual variables in the design, [44,79,80,82]. Maintaining pairwise orthogonality helps in achieving accuracy when performing integration via, e.g. the Monte Carlo type of method.

In some analyses it is beneficial when the design is "non-collapsible", i.e. lower-dimensional projections of the design points do not lead to replications. *Noncollapsibility* is important for situations when a design parameter (or input variable) has no influence. In such a case, two design sites that differ only in that parameter collapse; that is, the same design site is evaluated twice. This is clearly not desirable because the sparsity-of-effects principle is common in almost all systems. Sometimes, the goal of the design is to ensure that projections of the design are evenly distributed over selected subspaces. By doing this, one can obtain a small integration error if the chosen subset matches the leading terms in the ANOVA functional decomposition. Experience has shown that functions defined over many variables but with a low "effective dimension" in ANOVA decomposition often arise in practical applications [36,68].

Noncollapsibility can be achieved by, e.g. by restricting designs to the class of *Latin Hypercube* (LH) designs [7]. LH sampling (LHS) is also considered a *variance reduction technique* as it often decreases the variance of the estimator in Monte Carlo integration compared to simple random sampling.

1.1. Motivation and problem description

The ability to select uniformly distributed point sets/layouts from a design domain that satisfy most of the above-mentioned criteria has the potential to increase the efficiency of many engineering and scientific computations, as well as to improve the quality of engineering products and processes. In this paper, it is assumed that the domain within which either the integration, optimization, sensitivity study or other types of analyses are to be performed is normalized to a *design domain* $\mathscr{U} = [0, 1]^{N_{\text{var}}}$, i.e. a N_{var}-dimensional unit hypercube. The task is to select a design (a *sampling plan*) $\mathscr{D} \subset \mathscr{U}$, which is a table of N_{sim} points with N_{var} coordinates. The table consists of distinct input sites $\mathscr{D} = \{\boldsymbol{u}_1, \boldsymbol{u}_2, ..., \boldsymbol{u}_{N_{\text{sim}}}\}$ that are uniformly distributed. The notion of uniformity, although intuitively acceptable, does not have a single mathematical definition. In this paper, designs are meant to be uniform in two different ways, i.e. they should exhibit:

- *statistical uniformity*, meaning that any location (point) from the design domain must have the same probability of being selected. This is absolutely necessary for the Monte Carlo integration of a function featuring random variables sampled from $\mathscr{D}$ by inverse transformation of the cumulative distribution function,
- *sample uniformity*, meaning that each single point layout is *spread* uniformly throughout the design domain, i.e. the points must have a kind of equal spacing among them. Designs that enjoy sample uniformity are often called *uniform designs*, i.e. *low discrepancy* designs [48].

The simultaneous fulfillment of *statistical uniformity* and *sample uniformity* with *maximum projection regularity* (noncollapsibility) is assumed to be a sufficient condition for an *optimal* design.

We show that *sample uniformity* can be effectively achieved by an appropriate distance-based criterion, such as Maximin, miniMax, ϕ_p or Audze-Eglājs. However, *statistical uniformity* is known to be violated when using many standard criteria for sample optimization (either correlation or distance-based) [12,83]. The problem arises from the presence of the boundaries of the design domain. An elegant remedy that removes the problem by redefining the metric featured in the distance-based criteria has recently been suggested and shown by the authors to be an effective solution [12,83]. The present paper will employ this metric, which effectively makes the design domain *periodic*.

It was reported earlier in [21] that using a single criterion for selecting experimental designs for surrogate construction may lead to small gains in that criterion at the expense of large deteriorations in other criteria. Constructing designs by combining multiple criteria reduces the risk of using a poor design. The authors believe that using the proposed combination of a proper distance-based criterion and the assumption of the periodicity of the design space leads to robust and universal designs that perform well with respect to various other optimization criteria.

The point sets, $\mathscr{D}$, are obtained here by exploiting the analogy between an N-body system and a distance-based criterion of design optimality. A robust dynamical model capable of simulating N_{sim} points interacting within the periodic space of arbitrary dimension N_{var} is derived and presented. After the kinetic energy of the system dissipates due to damping, the positions of the particles in a steady-state equilibrium are treated as experimental points (the design). The performance of such designs is demonstrated in various contexts and applications and is compared to other existing strategies.

2. Distance-based criteria

Geometric criteria based on distance either measure only the distances amongst the points in the design, $\mathscr{D}$, or may consider the distances to all points in the domain $\mathscr{U}$. In any case, one has to define a proper norm (metric) $d(\boldsymbol{x}_i, \boldsymbol{x}_j)$ providing the "distance" between any points $\boldsymbol{x}_i, \boldsymbol{x}_j \in \mathscr{U}$.

First, one can consider a design that aims to achieve a high spread solely amongst its support points $\mathscr{D} \in \mathscr{U}$. when seeking such a design, one must attempt to make the smallest distance between the neighboring points in $\mathscr{U}$ as large as possible. This is ensured by the Maximin criterion

$$\phi_{\text{Mm}}(\mathscr{D}) = \min_{i \neq j} d(\boldsymbol{x}_i, \boldsymbol{x}_j) \qquad 1 \leq i, j \leq N_{\text{sim}} \tag{1}$$

A design that maximizes this measure is said to be a *Maximin* (Mm) distance design [29], denoted as $\mathscr{D}_{\text{Mm}}$. In an intuitive sense, $\mathscr{D}_{\text{Mm}}$ designs guarantee that no two points in the design are "too close", and

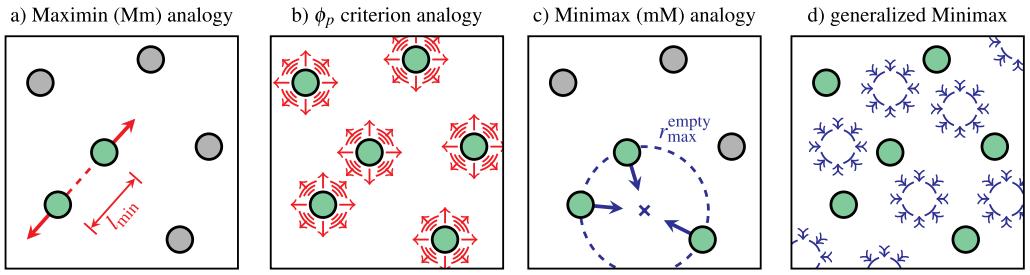

Fig. 1. Illustrations of various design criteria and the analogies with N-body systems in $[0, 1]^2$: repulsive point sets (a,b) and attractive empty regions (c,d). (a) Maximin criterion, (Eq. (1)), (b) generalization of the Maximin criterion (ϕ_p and Audze-Eglājs criteria, Eqs. (2) and (3)), (c) miniMax criterion, (Eq. (A.1)), (d) generalization of the miniMax criterion (Eq. (A.2)).

hence that the design points are spread over $\mathscr{U}$. The Maximin objective for the choice of points was first shown to be useful by Niederreiter [45]. Johnson et al. [29] illustrated the meaning of maximizing Eq. (1) using an analogy to the problem of spreading franchises (or the maximum facility dispersion problem [13]). Every franchise wishes to operate over its largest possible "exclusive territory", and therefore each of them can be thought to be active in *repelling* the other points (franchises), see Fig. 1a. The Maximin design emphasizes the non-redundancy in the choice of sites within the domain $\mathscr{D}$ and prefers designs suitable for Kriging as these have a sort of D-optimality property under certain conditions [29,31].

The Maximin criterion can be viewed as a limiting case of a more general criterion proposed by Morris and Mitchell [44], the ϕ_p criterion

$$\phi_p = \left(\sum_{i \neq j}^{N_{\text{sim}}} [d(\boldsymbol{x}_i, \boldsymbol{x}_j)]^{-p} \right)^{\frac{1}{p}} \tag{2}$$

where p is a positive integer. For a fixed metric, d, and a power, p, an N_{sim}-point design $\mathscr{D}_\phi$ is optimal if it minimizes the criterion in Eq. (2). This relaxed version of the Maximin criterion considers all interpoint interactions, as illustrated in Fig. 1b. The ϕ_p family of distance-based criteria has become very popular for comparison and selection between existing designs and is frequently used in research and in industry. It is also implemented in various software packages (e.g. MATLAB and R).

Note that taking the power $p = 2$ and the Euclidean intersite distance between all pairs of points leads to the Audze-Eglājs (ϕ_2) criterion [2]. Roshan and Hung use the power $p = 15$ in [31]. Some authors advise using powers as high as $p = 50$ combined with the Manhattan distance [28,59,78]. Taking $p = \infty$ renders the ϕ_p criterion equivalent to the Maximin criterion, Eq. (1). According to a recent paper [40], the power p should be dependent on the dimension of the problem, N_{var}. A simple analysis yields that the influence of long distances is sufficiently suppressed in favor of short distances when the power, p, exceeds the critical value, which is the domain dimension, N_{var}. Therefore, we recommend taking $p = N_{\text{var}} + 1$.

Now let us consider designs that attempt to *minimize* the maximum distance from all possible points in $\mathscr{U}$ to their closest point in $\mathscr{D}$. This is achieved by minimizing the miniMax criterion; see the illustration sketched in Fig. 1 c. This is another class of distance-based criteria which was introduced in [29], and was also motivated by the need to select an optimal design for Kriging. The miniMax criterion is described in more detail in this paper in Appendix A, together with the possibility of relaxing it (see Fig. 1 d) in the same manner as the Maximin was relaxed into the ϕ_p criterion. Appendix A also discusses the possibility of making an analogy between the relaxed miniMax criterion and an N-body system of particles.

Due to the reasons described in Appendix A, the ϕ_p criterion has been selected for exploitation as a template for the energy potential of an N-body system. For the derivation presented below, the original definition of the criterion in Eq. (2) is simplified by omitting the root '1/p', as it is a monotonous transformation that unnecessarily complicates the derivations and slows down computations. These two simplifications do not alter the inequalities whcih arise when comparing two designs. The redefined criterion reads (p remains a positive integer exponent, and $\boldsymbol{x}_i, \boldsymbol{x}_j \in \mathscr{D}$)

$$\phi_p = \sum_{i \neq j}^{N_{\text{sim}}} \frac{1}{d^p(\boldsymbol{x}_i, \boldsymbol{x}_j)} \tag{3}$$

2.1. Periodicity of the design space

The distance-based criteria presented in [29] were motivated by metamodeling rather than the need to select designs suitable for Monte Carlo integration. Therefore, they are not guaranteed to be *statistically uniform*. This paper uses the periodic metric proposed in [12,83] to maintain the *statistical uniformity* of the designs.

First of all, we limit our attention to the Euclidean distance metric. This metric is arguably much desired for its property of directional independence, or isotropy. The Euclidean distance between points i and j in N_{var}-dimensional space, L_{ij}, can be expressed as a function of their coordinates

$$L_{ij} = \sqrt{\sum_{v=1}^{N_{\text{var}}} (x_{i,v} - x_{j,v})^2} = \sqrt{\sum_{v=1}^{N_{\text{var}}} (\Delta_{ij,v})^2} \tag{4}$$

where $\Delta_{ij,v} = |x_{i,v} - x_{j,v}|$ is the difference in their positions projected onto the axis v.

As argued in [12,83], the natural choice of *intersite* Euclidean distance (a distance measured within $\mathscr{U}$) leads to a problem related to the boundaries of $\mathscr{U}$. To remedy this problem, a periodic extension of the design space has been proposed [12,83]. It is obtained simply by replacing $\Delta_{ij,\,v}$ in Eq. (4) with its periodic variant $\overline{\Delta}_{ij,v}$. The obtained metric, called the periodic length $\overline{L}_{ij}$, becomes the actual shortest linear path between point i and the nearest image of point j [12,83], also see Fig. 2.

$$\overline{L}_{ij} = \sqrt{\sum_{v=1}^{N_{\text{var}}} (\overline{\Delta}_{ij,v})^2} \qquad \overline{\Delta}_{ij,v} = \min(\Delta_{ij,v},\ 1 - \Delta_{ij,v}) \tag{5}$$

We note that using the nearest image of point j with respect to point i does not cover a true periodic repetition of the design domain. It only satisfies the *minimum image convention*. In a complete periodic repetition, an infinite number of images of point j would interact with point i. The presented approach is a simplification that has been shown in [12] to yield identical results to the fully repeated system in cases when the number of points, N_{sim}, is sufficient. If not stated otherwise, we take the periodic metric for the ϕ_p criterion in Eq. (3): $d^p(\boldsymbol{x}_i, \boldsymbol{x}_j) \equiv \overline{L}_{ij}^p$.

3. The analogy to a physical N-body system

With the given distance-based criterion in Eq. (3) and the periodic metric in Eq. (5), one can proceed with optimizing the design layouts.

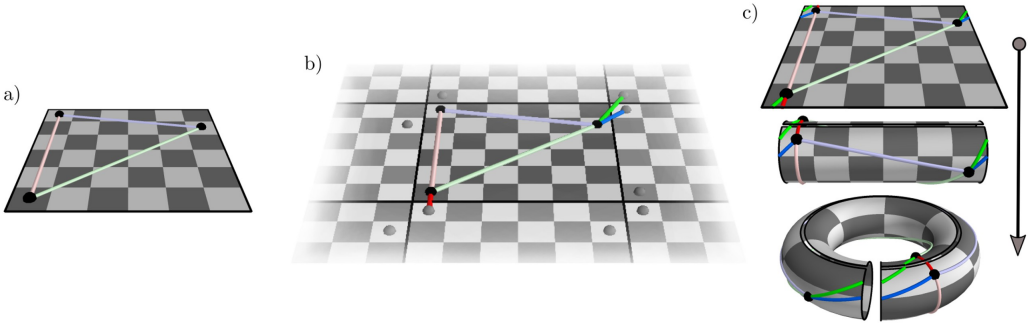

Fig. 2. Illustration of a periodically repeated planar domain. (a) the original two-dimensional design domain with pale-colored distances L_{ij} (Eq. (4)). (b) a periodically repeated design domain with eight additional images of each particle. The periodic distances $\overline{L}_{ij}$ (Eq. (5)) are dark-colored. (c) folding of the periodic domain into a torus.

One possible use of the ϕ_p criterion is for the comparison and selection of candidate designs, e.g. in some form of combinatorial or heuristic optimization of mutual ordering for a fixed set of coordinates [12,82].

This work proposes to interpret the distance-based ϕ_p criterion as the amount of potential energy stored within all interactions of a system of interacting (mutually repelling) particles; see Fig. 1b for an illustration. This physically analogical problem is simulated using a discrete dynamical system of mutually repelling particles. The coordinates of the particles of the dynamical system after reaching static equilibrium (after the minimization of potential and kinetic energy) may then be directly understood as the coordinates of design points within the unit hypercube.

We follow with the derivation of *equations of motion* of the dynamical (N-body) system. The derivation is conducted using Lagrangian mechanics. The Lagrangian $\mathcal{L}$ of the system can be described as follows

$$\mathcal{L} = E_k - E_p \tag{6}$$

with the *kinetic energy* of the particle system, E_k, being a simple sum of the kinetic energies of all particles of equal mass m

$$E_k = \frac{1}{2} m \sum_{i=1}^{N_{\text{sim}}} \sum_{v=1}^{N_{\text{var}}} \dot{x}_{i,v}^2 \tag{7}$$

where $\dot{x}_{i,v} = \frac{\mathrm{d}}{\mathrm{d}t} x_{i,v}$ is the velocity of the ith particle in dimension v. Once damping is introduced in the system, the kinetic energy decays with time.

Eq. (3) is considered to represent the total *potential energy* of the system of N_{sim} interacting particles. It sums the energy contributions, E_{ij}, of all $\binom{N_{\text{sim}}}{2}$ pairs of particles and thus can be rewritten as the sum of potential energies of individual pairs

$$E_p = \sum_{i=1}^{N_{\text{sim}}-1} \sum_{j=i+1}^{N_{\text{sim}}} E_{ij} = \sum_{i=1}^{N_{\text{sim}}-1} \sum_{j=i+1}^{N_{\text{sim}}} \frac{1}{\overline{L}_{ij}^{p}} = \phi_p \tag{8}$$

and represents the value of the ϕ_p criterion to be minimized.

Furthermore, it is necessary to calculate the derivatives of Lagrangian $\mathcal{L}$ with respect to all state variables: the coordinates $x_{i,v}$ and velocities $\dot{x}_{i,v}$ of all particles in each dimension. Obeying Lagrange's equations of the second kind

$$\frac{\mathrm{d}}{\mathrm{d}t}\left(\frac{\partial \mathcal{L}}{\partial \dot{x}_{i,v}}\right) = \frac{\partial \mathcal{L}}{\partial x_{i,v}} \tag{9}$$

one can start with the assumption that, apart from the derivatives with respect to time, t, the kinetic energy E_k is further differentiable only with respect to velocities $\dot{x}_{i,v}$, while the potential energy E_p (Eq. (8)) is differentiable only with respect to coordinates $x_{i,v}$. Therefore, the left-hand side of Eq. (9) is rather easily obtainable

$$\frac{\mathrm{d}}{\mathrm{d}t}\left(\frac{\partial \mathcal{L}}{\partial \dot{x}_{i,v}}\right) = \frac{\mathrm{d}}{\mathrm{d}t}\left(\frac{\partial E_k}{\partial \dot{x}_{i,v}}\right) = m\,\ddot{x}_{i,v} \tag{10}$$

with $\ddot{x}_{i,v} = \frac{\mathrm{d}}{\mathrm{d}t}\dot{x}_{i,v}$ being the acceleration of the ith particle in the dimension v.

The right-hand side of Eq. (9) becomes

$$\frac{\partial \mathcal{L}}{\partial x_{i,v}} = \frac{\partial E_p}{\partial x_{i,v}} = \sum_{j\neq i}^{N_{\text{sim}}} \left(\frac{1}{\overline{L}_{ij}^{p+1}} \frac{\overline{\Delta}_{ij,v}}{\overline{L}_{ij}}\right) \tag{11}$$

The resulting equation of motion of the ith particle in the vth dimension as assembled from Eqs. (9)–(11) finally reads

$$\ddot{x}_{i,v} = \frac{1}{m} \sum_{\substack{j=1 \\ j\neq i}}^{N_{\text{sim}}} \frac{\overline{\Delta}_{ij,v}}{\overline{L}_{ij}^{p+2}} = \frac{1}{m} \sum_{\substack{j=1 \\ j\neq i}}^{N_{\text{sim}}} F_{ij,v} \tag{12}$$

The interaction of two particles i and j, together with the projections of distances, forces and accelerations, is illustrated in Fig. 3c. The motion of the dynamical system is therefore described by a system of independent equations. Awareness of this is of high importance while considering the possibilities for a solution method and its computer implementation. It means that the accelerations $\ddot{x}_{i,v}$ of each particle

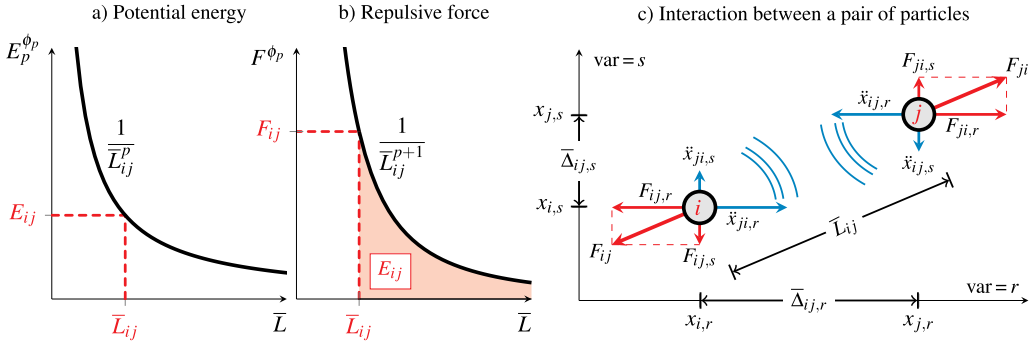

Fig. 3. Interaction of a pair of particles. (a) Potential energy. (b) Repulsive force acting on particles. (c) Components of repulsive force and acceleration.

$i = 1, \ldots, N_{\text{sim}}$, in each dimension $v = 1, \ldots, N_{\text{var}}$, can be solved separately without solving a system of equations. The damping of the motion of particles also depends solely on the velocity of each particle, see below. Furthermore, each distance projection $\overline{\Delta}_{ij,v}$ as well as each absolute distance $\overline{L}_{ij}$ can be computed independently. The above-mentioned properties lead to the possibility of utilizing a *parallel* implementation. The parallel computer implementation of the presented dynamical system using a GPU has been thoroughly described in [41].

As soon as the new accelerations of each particle in each dimension are obtained, the equations of motion are numerically integrated using the semi-implicit Euler method and the new velocities $\dot{x}_{i,v}$ and coordinates $x_{i,\ v}$ of each particle in each dimension at the new time $(t + \Delta t)$ are computed

$$\dot{x}_{i,v}(t + \Delta t) = \dot{x}_{i,v}(t) + \Delta t \cdot \ddot{x}_{i,v}(t) \tag{13}$$

$$x_{i,v}(t + \Delta t) = x_{i,v}(t) + \Delta t \cdot \dot{x}_{i,v}(t + \Delta t) \tag{14}$$

Note that these are equations of motion of a conservative dynamical system as defined by the energy potential Eq. (6), which does not cover any form of energy dissipation. In order for a dynamical system to reach static equilibrium, implementation of energy dissipation is desirable. Various types of damping are typically combined. To solve the problem at hand, we add the sum of velocity-dependent damping members to Eq. (14): $\sum_q c_q \dot{x}_{i,v}^q(t)$, where c_q are damping coefficients and q are various powers of the velocity, $\dot{x}_{i,v}$, of the ith particle in the vth dimension. The damping part is not derived from the energy potential of the particle system but is introduced artificially.

A question may arise about the forces acting on each pair of particles. By differentiating the energy potential ($E_{ij} = 1/\overline{L}_{ij}^p$, Fig. 3a) with respect to the distance, $\overline{L}_{ij}$, the *repulsive* force F_{ij} is obtained: $F_{ij}(\overline{L}_{ij}) \propto 1/\overline{L}_{ij}^{p+1}$; Fig. 3b. The formulation of this force as a scale-independent power law is very much desired for obtaining self-similar point patterns. Numerically however, during the dynamical simulation the mutual repulsive force between two very close particles tends to infinity (or beyond the numerical range), leading to an ill-posed problem.

The remedies for such unwanted behavior for the numerical solution of an N-body system can be found in the field of astrophysics simulations of collisionless bodies, see e.g. [1]. It is often proposed to use a *softening factor,* λ; this is a term that introduces a cross-over distance between two power-law asymptotes: $F_{ij}^{(\lambda)} = 1/(\overline{L}_{ij}^2 + \lambda^2)^{(p+1)/2}$. Here the cross-over distance λ is selected as $\lambda \ll \ell_{\text{char}}$, where ℓ_{char} is the characteristic length (roughly the average distance between neighboring particles for uniformly spread points, see the definition in Eq. (15)). The introduction of such a smooth softening causes the force to be bounded from above by the left asymptote: $F_{\max}^{(\lambda)} = 1/\lambda^{p+1}$ for $\overline{L}_{ij} = 0$ and to converge to the right asymptote that is the original power law for $\overline{L}_{ij} = \infty$. However, the enforcement of a function other than the derived power law $1/\overline{L}_{ij}^{p+1}$ is undesired as it distorts the ratio between repulsive forces in the resulting steady state. Therefore, the resulting optimized point patterns do not entirely obey the ϕ_p criterion.

The most convenient remedy here is to graft a constant function onto the interaction law for distances below λ_{cst} ($\lambda_{\text{cst}} \ll \ell_{\text{char}}$). That way, if the pairwise distance is greater than λ_{cst}, the proposed power-law interaction is used as is. Once the mutual distance between particles becomes lower than λ_{cst}, the repulsive force remains constant $F_{\text{cst}}^{(\lambda)} = 1/\lambda_{\text{cst}}^{p+1}$. Unlike the astrophysics systems of moving bodies, the purpose of the N-body system in this work is to find a steady-state solution that minimizes the potential energy of the system. The trajectory that leads to such a solution is considered to be of no interest. For these static-equilibrium states (point patterns) one can assume that the shortest pairwise distances within such patterns are about the length of ℓ_{char}. It is therefore crucial to preserve the power law interaction at least to this threshold. To be on the safe side, let us require $\lambda_{\text{cst}} = \ell_{\text{char}}/10$. Any changes in particle interaction below this limit will not spoil the desired point patterns but will prevent the accelerations from approaching infinity.

For the purposes of the actual numerical simulation of the dynamical system, a unitary mass, $m = 1$, is used for all bodies. Even though the equations of motion Eq. (12) do not contain any kind of "stiffness coefficient", for convenience we propose that all the repulsive forces be divided by the number of point pairs (interactions), $\binom{N_{\text{sim}}}{2}$. This normalization of the repulsive forces helps to tame the enumerated forces when simulating increasingly more saturated systems, especially near steady-state configurations. During the optimization of the point samples used in this work, the time step of the numerical integration was set to 0.005 s.

4. Remarks on the properties of the designs obtained by the proposed DYN scheme

The designs obtained by the proposed numerical simulation of a dynamical system in a periodic domain have some specific properties.

• The first remark deals with the difference between the standard *intersite metric* and the *periodic metric* proposed recently by the authors [12,83]. This concerns not only the proposed DYN method but also distance-based criteria in general. The standard way of measuring the distance between two points is naturally to take the distance *within* the design domain. Some authors believe that the Maximin or ϕ_p criterion "spreads out its points evenly over the design region" [10,11]. We, however, argue that designs optimized with the ϕ_p or Mm criterion do *not* cover domains uniformly, see e.g. Fig. 4a. This nonuniformity was also noticed by Santner et al. [65]. However, the same authors suggest that one should "remedy this by restricting the class of available designs to only include, say, LHDs". We argue that using LH-sampling *does not* help in the achievement of statistically uniform designs [12,83] (LH-Mm or more generally, LH-ϕ_p designs), i.e. the attainment of equal probability for any location in $\mathscr{U}$. Indeed, as shown [12] in the case of the Audze-Eglājs criterion, LH designs with an intersite distance metric have nonuniform point occurrence density in $\mathscr{U}$. From here on, analyses will only be performed with the *periodic* metric.

• The experience with DYN designs is that they tend to form a kind of regular arrangement with preferential orientation whenever possible. These regular arrangements can only be formed for selected combinations of point counts and domain dimensions. When the point count is

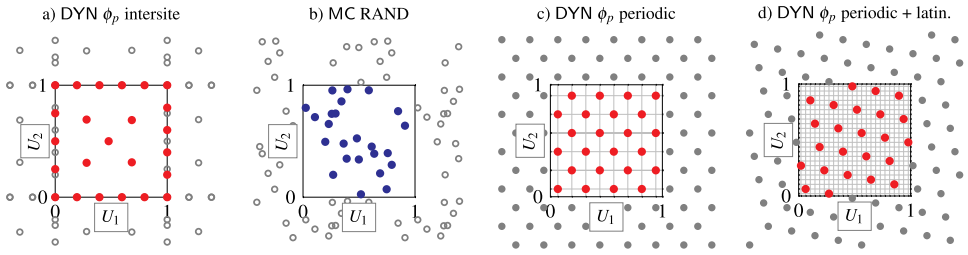

Fig. 4. Illustration of the optimization process of $N_{\text{sim}} = 24$, $N_{\text{var}} = 2$ (with part of the surrounding periodically repeated domain). The initial random arrangement is (b). The intersite ϕ_p criterion leads to the design (a). The periodic ϕ_p criterion yields a collapsible pattern (c) which is further "latinized" (d); see below for an explanation of the latinization process.

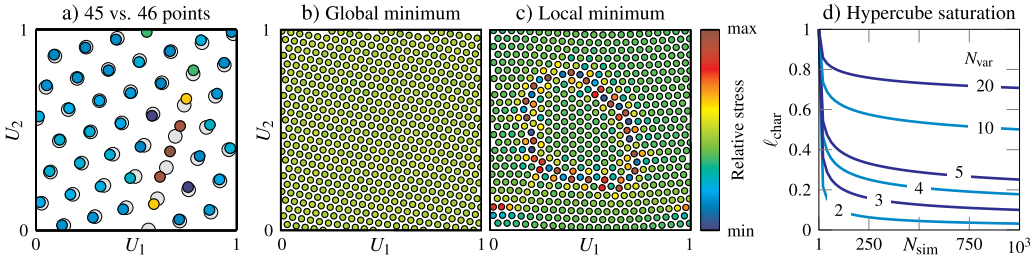

Fig. 5. Properties of DYN designs. (a) Difference between $N_{sim} = 45$ (gray circles) and 46 points (circles colored with a kind of "stress") in 2D. (b) and (c) Global and local minimum configurations for $N_{sim} = 560$ points in 2D. (d) Characteristic length as a function of point count in various dimensions.

high enough and only slightly exceeds the point count needed for a perfect regular pattern, systems tend to locally "squeeze" an additional point into the otherwise regular arrangement; see Fig. 5a, where 45 points form a regular pattern whereas 46 points enforce an additional point by locally rearranging the pattern.

• The reason this kind of directional preference is observed (see Fig. 5 a,b) is that the periodic metric depends on the directions of individual variables even though it is based on the isotropic Euclidean metric. Indeed, the min operation in Eq. (5) is performed in each individual direction. As a result, the distance between a pair of points depends on the orientation of the vector that connects them.

• In some cases (selected combinations of N_{sim} and N_{var}), the designs form regular patterns that are aligned with one or more hypercube edges, see Fig 4c. In this case the design is collapsible, which may not be desirable. To avoid this exhibition of collapsibility by dynamically optimized samples, we propose that the dynamical optimization be performed as described above, with the possible collapsibility being post-processed (rectified) afterwards. A convenient approach is to perform the *latinization* of samples, meaning the sorting and rearrangement of the coordinates of sampling points in the sense of the LHS method. In other words, each sampling point is translated along each dimension to the center (strata median, see [82]) of the closest LHS cell with the coordinates: $x_{i,v}^{\mathrm{LHS}} = (\pi_i - 0.5)/N_{sim}$, where the integer rank π_i is a permutation of $i = 1, 2, \ldots, N_{sim}$.

The problem with collapsible samples is that if multiple points occupy an identical coordinate, ordering these identical numbers essentially randomizes the design. Superior results can be obtained if the sample is slightly pre-rotated along each axis. We propose an empirical value for this rotation of about $\mathrm{arctg}(\ell_{char})/4$ in a random direction. By performing such a rotation about each axis, the subsequent latinization yields well distributed LH samples, see Fig. 4d. We remark that this latinization via post-processing may not necessarily provide the best possible LH sample for a given ϕ_p criterion. However, the latinization of a DYN design is much faster than combinatorial optimization, which operates on predefined coordinates by "shuffling" [82].

• A different option for the removal of perfect regularity is to introduce dry friction damping into the dynamical simulation. Alternatively, use can be made of any other source of random error/irregularity that makes the design pattern more "organic" and yet does not violate the uniformity too much.

• Another issue is the (in)ability to find a perfect configuration corresponding to the global minimum of the potential energy in domains highly saturated with particles. Fig. 5b and 5c show almost identical designs with $N_{sim} = 560$ points in two dimensions. The point arrangement in Fig. 5b represents the perfect global minimum configuration. The arrangement on the right represents a near-optimal layout according to potential energy. The amount of potential energy stored in both systems (b) and (c) is nearly identical, as is their performance in Monte Carlo integration. However, by comparing the amount of relative radial stress acting upon each particle it is possible to reveal inhomogeneities that divide regions with different directional alignments.

• Essentially, the problem is similar to, e.g. the annealing and controlled cooling of optical glass to ensure the uniformity of its refractive index [39]. At the beginning of a dynamical simulation with randomly distributed particles there is more than enough of kinetic energy to agitate the bodies and overcome any local potential energy minimum. It is very desirable to set the overall damping low enough to provide the moving bodies with enough kinetic energy and time to arrange themselves into the optimal steady-state layout corresponding to the global potential energy minimum. In fact, there seems to be no lower bound on minimum damping. The lower the overall damping is set, the lower the probability of attaining a near-optimal, inhomogeneous, design. Naturally though, lower damping induces a slower dissipation of energy, resulting in greater simulation duration. The importance of this requirement, nevertheless, only becomes pronounced for very high design domain saturations. At that point, however, the emergence of irregularities does not make much of a difference to the global minimum, relatively speaking. During the optimization of the point samples used in this work, it was found to be sufficient to use viscous linear damping set to 0.025 only.

• The last remark deals with the average density of points in the unit hypercube, $\mathscr{U}$. We quantify the *saturation* of the design domain by the *characteristic length*

$$\ell_{char} = \frac{1}{\sqrt[N_{var}]{N_{sim}}} \tag{15}$$

The physical meaning of ℓ_{char} is the average distance between neighboring points when they are uniformly spread over $\mathscr{U}$. Eq. (15) can be illustrated well using a regular orthogonal grid with $N_{sim} = N^{N_{var}}$, where N is the number of equispaced 1D projections of the grid and $\ell_{char} = 1/N$. Uniformly distributed designs in various dimensions achieve a similar saturation when ℓ_{char} is similar. It becomes increasingly harder to achieve the required ℓ_{char} as the dimension, N_{var}, increases because the space to fill becomes too large. Fig. 5d shows how the characteristic length decreases with an increasing number of points for various dimensions.

5. Numerical examples

In this section, the performance of designs obtained with the proposed dynamical algorithm (DYN) is critically assessed and compared to other existing sampling schemes. Several contexts are selected to report the performance of the designs: estimation of the global extreme of a function over $\mathscr{U}$, estimation of an integral of a function (estimation of the average), estimation of the standard deviation of a function of a random vector, and estimation of the failure probability of a truss using a combination with Importance Sampling (IS). The competing reference approaches are crude Monte Carlo (MC), Quasi Monte Carlo (QMC) sequences, randomized Quasi Monte Carlo (RQMC) sequences and Latin Hypercube Sampling (LHS) with randomly ordered samples.

The problems are analyzed in various dimensions, N_{var}, and the study is always performed for a series of different sample sizes, N_{sim}. Since the designs are not unique (apart from QMC), the target estimated values are viewed as random variables. As such, the results are always obtained by running the problem N_{run} times and reporting the estimated results via their averages (ave) and sample standard

deviations (ssd). This treatment enables the *variance* of the estimators to be reported; it is preferred that this variance be minimized in practice. Plots of performance have the target parameter as ordinate and the sample size, N_{sim}, as abscissa.

Before presenting the results, a brief review of the techniques under comparison is presented.

Quasi Monte Carlo sequences, which are sometimes named *low-discrepancy sequences* or *digital nets*, have been developed for multi-dimensional integration. Examples of these are the sequences by Halton [23] (generalizations of the one-dimensional van der Corput sequence), Sobol' [70,71], Niederreiter [46,47,49], Faure [17] and the generalization of the Faure sequence by Tezuka [76], and others. QMC methods are called "number-theoretic methods" [14,15] by some authors (e.g. "good lattice points", etc.). QMC sequences have become famous for their ability to decrease the variance of estimation of integrals in comparison with crude Monte Carlo integration, as well as to increase the speed of convergence of the integral estimate [34,57]. The central theorem of the classical part of the theory of uniform distribution, in connection with the Riemann integral criterion, is Weyl's criterion [84]. It is strongly connected to the notion of discrepancy. The use of low-discrepancy sequences forms a cheap alternative to algorithmic *discrepancy minimization* [48, Chapters. 3 & 4].

QMC methods may be thought of as derandomized Monte Carlo samples. It has become apparent that QMC can be re-randomized (RQMC) in order to obtain sample-based error estimates. Various re-randomization methods have been developed (e.g. random shift modulo one [9], scrambling by Owen [56], and others). These randomizations are also known to have better projection properties then some digital nets (e.g. Sobol') to the first few dimensions [34], see below. Surveys of RQMC appear in [34,57].

Another method selected for comparison is Latin Hypercube sampling. LHS is especially suitable for evaluating the *expectation of functions* in computer experiments. LHS can be viewed as a stratified sampling method as it operates by subdividing the sample space into smaller regions and then sampling within these regions. This procedure creates samples that more effectively fill the sample space. When the analyzed transformation has suitable properties, the variance of the LHS-based estimators is drastically reduced compared to simple random sampling (LHS is a *variance reduction technique*). Indeed, LHS has repeatedly been reported to provide a smaller asymptotic variance for the sample mean compared with simple random sampling. Several authors have focused on the characterization of sampling efficiency for LHS. LHS have been found to be efficient especially in the statistical analysis of functions of variables that are additive, have low interactions and are monotonous transformations of individual variables [43,54,68,72]. LHS has become very popular and has been applied to nearly every type of probabilistic analysis: see, e.g. its application to the estimation failure probability [50,53], coefficient estimation for polynomial chaos [4], neural networks [51], and other types of surrogate models [19,20]. The popularity of LHS has led to the invention of numerous variants intended to improve space-filling [3,6,12,18,29,31,44], optimize its projective properties [26,38], minimize least square error and maximize entropy [58], and reduce spurious correlations [6,27,55,75,80,82]. There are even variants providing various ways to extend the sample size [64,69,77,81].

5.1. Extremes and averages of a moving mean – comparison with QMC and RQMC

In this numerical example a function is selected and defined over $\mathscr{W}$. The target is to estimate the extreme of this function and also the integral over this function (an operation related to averaging). The maximum over the design domain, E, is estimated as $\hat{E}$ using a single design $\mathscr{D} \in \mathscr{W}$. Similarly, the exact value of the integral, I, is estimated using the average, $\hat{I}$, evaluated using a single design $\mathscr{D} \in \mathscr{W}$

$$E = \max_{\boldsymbol{x}\in\mathscr{W}} f(\boldsymbol{x}) \qquad \hat{E} = \max_{\boldsymbol{x}_i\in\mathscr{D}} f(\boldsymbol{x}_i) \tag{16}$$

$$I = \int_{\mathscr{W}} \dots \int f(\boldsymbol{x})\mathrm{d}\boldsymbol{x} \qquad \hat{I} = \frac{1}{N_{\text{sim}}}\sum_{i=1}^{N_{\text{sim}}} f(\boldsymbol{x}_i) \tag{17}$$

The following testing function has been selected for the evaluation of the performance of the designs in N_{var}-dimensional space

$$f(\boldsymbol{x}) = \exp\left[-\left(\frac{d(\boldsymbol{x},\boldsymbol{c})}{\ell_{\text{char}}}\right)^2\right] = \exp\left[-\sum_{v=1}^{N_{\text{var}}}\left(\frac{\overline{\Delta}_{xc,v}}{\ell_{\text{char}}}\right)^2\right] \tag{18}$$

where $d(\boldsymbol{x}, \boldsymbol{c})$ is the *periodic* distance between a point $\boldsymbol{x} \in \mathscr{W}$ and the function "center", $\boldsymbol{c} \in \mathscr{W}$. This periodic distance follows the definition in Eq. (5), i.e. the squared periodic distance reads $d^2(\boldsymbol{x}, \boldsymbol{c}) = \sum_{v=1}^{N_{\text{var}}} (\overline{\Delta}_{xc,v})^2$, where the periodic projections of distance between $\boldsymbol{x}$ and $\boldsymbol{c}$ are computed using the actual projections, $\Delta_{xc,v} = |x_v - c_v|$, as $\overline{\Delta}_{xc,v} = \min(\Delta_{xc,v},\ 1 - \Delta_{xc,v})$. This function may be usable as the autocorrelation function of a random field: in its present form it is the squared exponential autocorrelation function, separable (multiplicative) and isotropic, with ℓ_{char} being the autocorrelation length. The function (a smooth bell-shaped or "Gaussian" function) is depicted in Fig. 6 bottom right. The length scale has been deliberately selected so that it is dependent on the sample size. One may think of its discretization by $\boldsymbol{x} \in \mathscr{W}$ as a crude and economical approximation of the function. Any defect in the design (either a cluster of points or an empty region) may cause the estimation to deteriorate.

The center of the bell-shaped function, $\boldsymbol{c}$, is shifted randomly in all possible directions. Thanks to the periodic distance, the part of the function that "overlaps" the domain appears from the other side. In this way, both the exact peak value and the integral remain constant independently of the random shift. The exact peak value of the function is attained at the center $\boldsymbol{c}$ and equals one. The exact value of the integral can also be solved analytically

$$E = 1 \tag{19}$$

$$I = \int_0^1\int_0^1\int_0^1 \dots \int_0^1 \exp\left[-\sum_{v=1}^{N_{\text{var}}}\left(\frac{x_v - 1/2}{\ell_{\text{char}}}\right)^2\right]\prod_{v=1}^{N_{\text{var}}}\mathrm{d}x_v = \left[\ell_{\text{char}}\sqrt{\pi}\,\mathrm{erf}\left(\frac{1}{2\ell_{\text{char}}}\right)\right]^{N_{\text{var}}} \tag{20}$$

where $\mathrm{erf}(\cdot)$ is the error function related to the Gaussian cumulative distribution function.

The numerical example features integration, a classical task for which QMC and RQMC have been developed. The sequences, just as with various improvements to MC such as stratification in LHS, are designed to improve the accuracy of integration to favorable functions while doing no harm for unfavorable ones. QMC methods are generally assumed to be the most efficient integration tool for smooth functions and are thought of as being the gold standard for numerical integration. However, as pointed out e.g. in [34], QMC methods are successful due to their clever choice of point sets in order to exploit the features of the functions that are likely to be encountered (such as various symmetries). They cover the main effects, diagonals, etc. We claim that such a "tuned" search must come at a price: the sequences may lose their efficiency if the function does not possess simple symmetries, etc. To test their robustness when integrating real-life functions, we evaluate the integral for N_g locations of the center, $\boldsymbol{c}$, arranged in a dense regular orthogonal grid in an attempt to exhaust all possible mutual shifts. The relative positions of the design points with respect to $f()$ change and therefore the (otherwise deterministic) results obtained with QMC can be processed as random variables.

To assess the performance of each single design in estimating either the integral I or the maximum E, the absolute difference between the exact solution and its estimation is divided by the exact solution

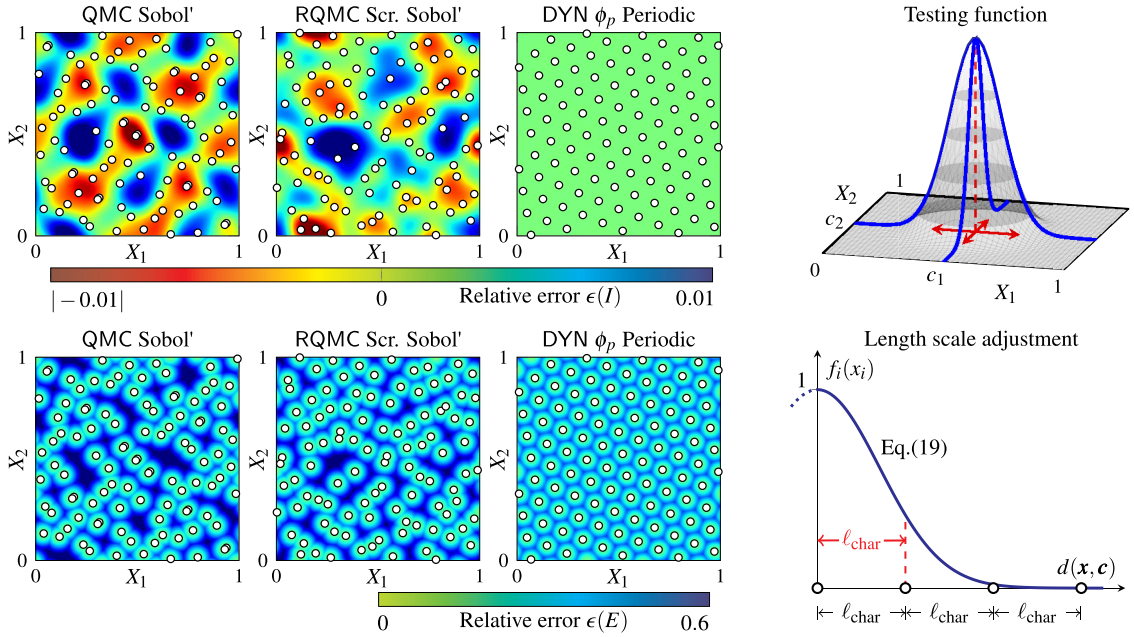

Fig. 6. Approximation of a bell-shaped function for $N_{\text{sim}} = 102$. Top row left: Error in approximation of the integral, $\epsilon(I)$. Bottom row left: Error in approximation of the maximum, $\epsilon(E)$. Top right: depiction of the "moving" function in two dimensions. Bottom right: illustration of the testing function in one dimension.

$$\epsilon(I) = \left| \frac{I - \hat{I}}{I} \right| \quad \text{and} \quad \epsilon(E) = \left| \frac{E - \hat{E}}{E} \right| \tag{21}$$

In particular, the errors $\epsilon(E)$ and also $\epsilon(I)$ in Eq. (21) are reported via their averages, 'ave', and sample standard deviations, 'ssd'. These statistics are computed using $N_{\text{run}} \times N_{\text{g}}$ realizations of an error (note that in the case of QMC and RQMC sequences there is just one run: $N_{\text{run}} = 1$).

The ave values are connected by a solid line in Fig. 7 and in Fig. 8 and plotted as functions of the sample size. Additionally, they are surrounded by a scatterband of $\pm$ one ssd in order to assess the variance of the estimation. Fig. 7 displays the ave and ssd of the absolute error value: $|\epsilon(I)|$ for the error in integration. In an ideal situation, both errors in Eq. (21) are equal to zero, with no scatter. Variations in error result from either having a different shift or a different run (sample set).

The graphs in Figs. 7 and 8 show that crude MC provides sample sets that produce large errors and also exhibit large variance. The picture is similar for any of the four dimensions of the design domain. Limiting the point sets to the LHS class improves the performance by both decreasing the ave error and decreasing the variance. The QMC (Sobol') sequences and also the RQMC (scrambled Sobol') sequences deliver a major improvement, as expected. These sequences, albeit repeatable (deterministic), still produce scatter due to the various shifts of the center $\boldsymbol{c}$ with respect to the point set. Note that keeping the center of the symmetrical testing function in the center of $\mathscr{U}$ would help QMC methods to show themselves in a better light, but the present example aims at testing the *robustness* of the designs. Finally, the results obtained with the proposed DYN samples greatly outperform those from all other techniques. The point sets are very robust, meaning that that the error has a small scatter and the ave error remains very small for any sample size.

To visually support the claim of *robustness*, we have selected one of many sample sizes for which the DYN technique delivers a perfect pattern that can be built from a small tile: $N_{\text{sim}} = 102$ for $N_{\text{var}} = 2$, see Fig. 6. The point sets are visualized by empty circles. The pattern resembles a "lattice point set". The three figures on the left show the dependence of both studied errors on the location of the center of the testing function (a kind of "influence line" similar to that known from structural analysis). The color at a certain location simply corresponds to the error when the function is centered at that location. One can see how much the QMC error is sensitive to the shifts while the DYN samples are insensitive. The DYN method forms a pattern that always

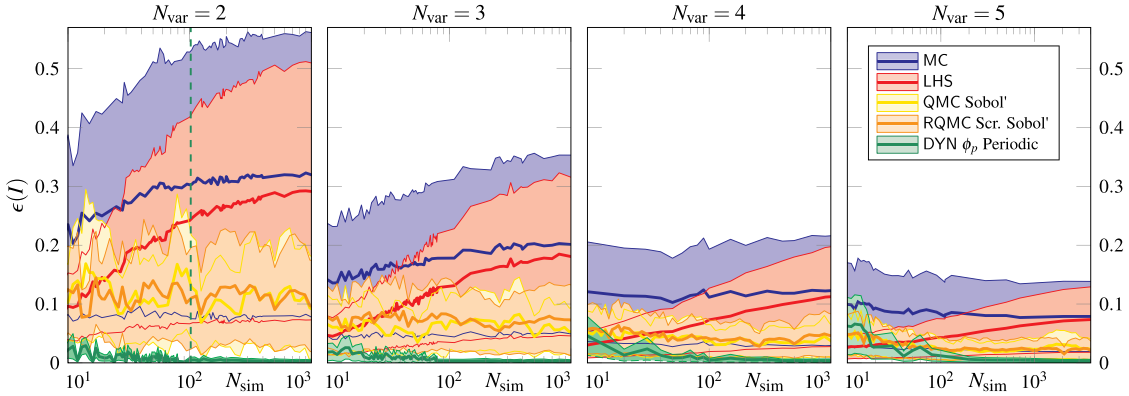

Fig. 7. Estimation error of the integral, $\epsilon(I)$, of the testing function from Eq. (18) plotted as a function of sample size N_{sim}. The solid lines represent the ave estimation and are surrounded by a band of $\pm$ ssd. The vertical line at $N_{\text{var}} = 2$ and $N_{\text{sim}} = 102$ indicates the designs studied in Fig. 6.

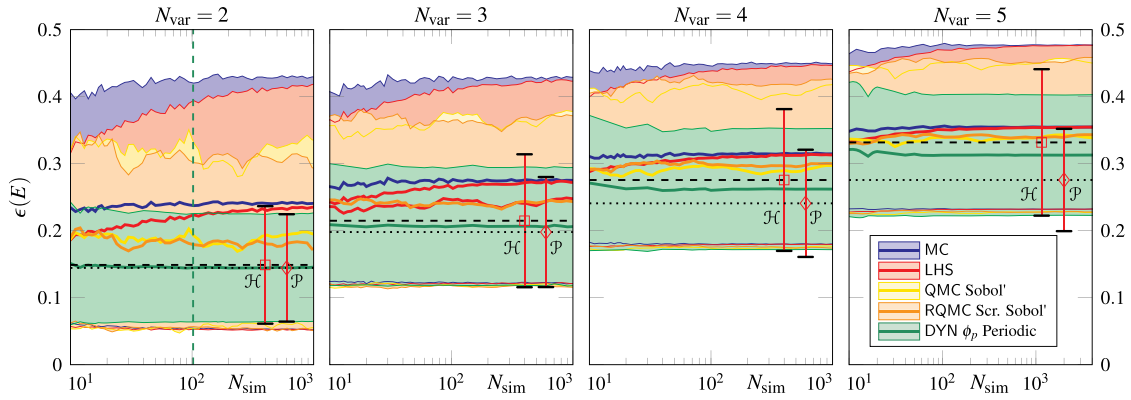

Fig. 8. Estimation error $\epsilon(E)$ of the extreme of the testing function from Eq. (18) plotted as a function of sample size N_{sim}. The solid lines represent the `ave` estimation and are surrounded by a band of $\pm$ `ssd`. The vertical line at $N_{var} = 2$ and $N_{sim} = 102$ indicates the designs studied in Fig. 6. (For interpretation of the references to color in this figure, the reader is referred to the web version of this article.)

delivers $\epsilon(I)$ error which is orders of magnitude smaller than that produced by QMC and also RQMC. The reason is the simultaneous *statistical uniformity* and *sample uniformity* of the DYN design.

We shall now comment on the ability to estimate the extreme of a function, which is measured via error $\epsilon(E)$, see Fig. 8. MC designs have `ave` errors starting for $N_{sim} = 1$ at the level marked by empty squares. These errors correspond to the random placement of a single point within a hypercube domain, or the use of a regular orthogonal grid as a point pattern (see Appendix B for the derivation for pattern "$\mathscr{H}$"). As the sample size increases, the average errors of the MC samples increase towards an asymptotic result. The same asymptote also holds for errors obtained with LHS designs. QMC and RQMC designs show better performance and the errors seem to be independent of domain saturation. Finally, DYN designs have `ave` and `ssd` values which are smaller compared to those of the other designs. The DYN designs also have `ave` and `ssd` values which are constant functions independent of domain saturation. This tells us that the designs form self-similar patterns that can be characterized by a smaller number of points (a small tile that effectively repeats throughout the domain). The statistics for the error obtained with MC and LHS show a trend and stabilize only after reaching a high degree of saturation. Theoretically, the best possible pattern corresponds to centers of regular polyhedral tessellation $\mathscr{P}$ (the points form a regular simplex grid), and the errors corresponding to it are marked by empty diamonds. Derivations are presented in Appendix B.

5.2. Sum of exponentials of normal variables – comparison with LHS

In this numerical example the ability to estimate the standard deviation of $g(\boldsymbol{X})$ – a deterministic function of a random vector, $\boldsymbol{X}$, is assessed. The standard deviation is estimated using N_{sim} points by a point estimator – the classical *sample standard deviation*, i.e. the square root of the average squared deviation from the mean value. The results of the proposed DYN designs are compared to QMC and RQMC sequences, and additionally to LHS.

The selected problem has been featured in [81] and also in [12] for evaluating the performance of LHS samples optimized by combinatorial optimization via the Audze-Eglājs criterion in a periodic design domain (periodic Audze-Eglājs – PAE). The random vector is taken as a Gaussian random vector with N_{var} independent standardized marginals: $X_v \sim \mathcal{N}(0, 1)$. The marginal random variables can therefore be obtained by component-wise inverse transformation of the cumulative distribution function (CDF), $x_v = \Phi^{-1}(u_v) = \sqrt{2}\,\mathrm{erf}^{-1}(2u_v - 1)$, where u_v are coordinates of the points in $\mathscr{U}$ (sampling probabilities) and erf is the error function. The studied example considers the function $g_{exp}(\boldsymbol{X})$

$$g_{exp}(\boldsymbol{x}) = \sum_{v=1}^{N_{var}} \exp(-x_v^2) \tag{22}$$

The exact mean value reads $\mu_{exp} = N_{var}/\sqrt{3}$ [81]. Since the function $g_{exp}(\boldsymbol{X})$ represents a sum of independent marginals, any LHS sample estimates the average with zero variance (the mutual ordering of LH-coordinates becomes irrelevant). We focus on the estimation of standard deviation

$$\sigma_{exp} = \sqrt{N_{var}}\sqrt{\frac{1}{\sqrt{5}} - \frac{1}{3}} \approx 0.337\,461\sqrt{N_{var}} \tag{23}$$

The convergence of this estimate is evaluated for sample sizes $N_{sim} = \langle 1, \ldots, 4096 \rangle$ in two and five dimensions. The results are presented in Fig. 9. Again, we plot the `ave` and `ssd` obtained using $N_{run} = 400$ runs – realizations of the design (note that $N_{run} = 1$ in the case of the QMC and RQMC sequences). All sampling techniques eventually tend

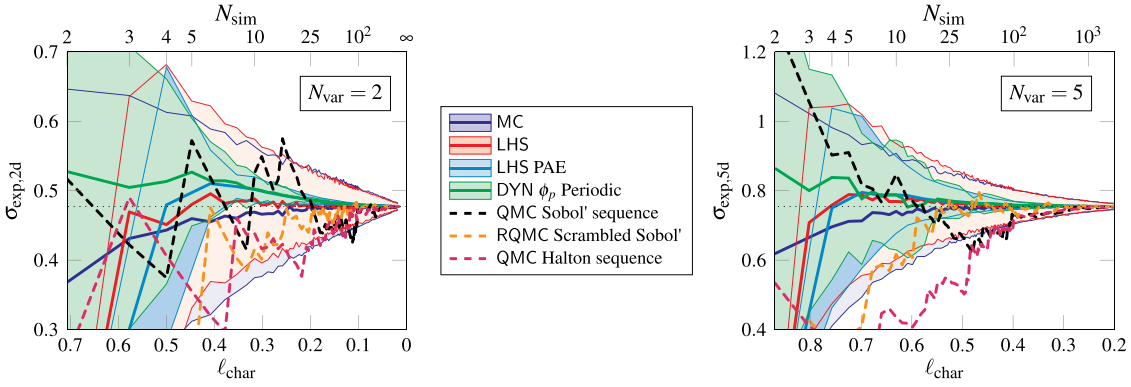

Fig. 9. Estimated standard deviation as a function of sample size (and characteristic length). Left: Two dimensions. Right: Five dimensions.

to an exact solution. MC has the highest variance (notice the wide scatterband around the average estimation). Restricting the designs to LHS does not improve the results much. The proposed DYN samples seem to provide a major improvement compared to the other sampling schemes: they provide unbiased results for very small sample sizes and yet their variance is very small. The reason for the absence of bias is that the samples are statistically uniform, and the small scatter can be attributed to the sample uniformity of the point sets. Additionally, the results obtained with QMC sequences (namely the Halton and Sobol' sequences) are presented. They have no scatter as there is always only one realization for a given N_{sim}. The zigzag profile of the estimation nicely demonstrates how the sequences consecutively fill various parts of the design domain. The comparable range for the behavior of DYN samples in various dimensions begins at around $\ell_{\text{char}} = 0.6$, which seems to be the critical particle saturation for the dynamical system to assemble meaningful patterns. We remark that the DYN results are comparable to the results obtained with LHS optimized via the PAE criterion using combinatorial optimization [12]. This is because both DYN and LHS-PAE use the same kind of distance-based criterion. However, it is much more computationally demanding to use combinatorial optimization than it is to solve the N-body dynamics. Finally, we remark that the results for latinized DYN samples are comparable to those obtained with LHS, and thus an LH-type design can be obtained relatively easily by postprocessing a DYN design.

5.3. Failure probability of a truss using a combination with IS

In this numerical example, the target is to estimate the failure probability of a truss structure (numerical model) using Importance Sampling (IS). The aim is to show whether there are differences in performance when the IS density, centered at the design point, is represented by various sampling schemes: DYN, LHS and MC.

The engineering application example is taken from [5,33,35], where it served as one of the benchmark problems for comparison of methods for estimating structural reliability. The setup of the numerical experiment is illustrated in Fig. 10.

The input random vector of the model, $\boldsymbol{X}$, consists of five random variables: the properties of the horizontal members (Young's modulus E_{h} and cross-section area A_{h}), the properties of the diagonal members (Young's modulus E_{d} and cross-section area A_{d}), and the magnitude of the loading forces P in the top joints. The properties of the input random variables are summarized in Table 1. Since the input random variables are independent, their distribution functions form a multivariate uniform distribution defined in $\mathscr{U} = [0, 1]^{N_{\text{var}}}$. Therefore, from now on we shall denote the variables of the real (physical) space by $\boldsymbol{X} = \{X_1, \ldots, X_{N_{\text{var}}}\}$ and the corresponding probabilities by $\boldsymbol{U} \in \mathscr{U}$, where $\boldsymbol{U} = \{U_1, \ldots, U_{N_{\text{var}}}\}$. Transformation between $\boldsymbol{U}$ and $\boldsymbol{X}$ is particularly simple as it is a set of component-wise transformations $U_v = F_v(X_v)$. The realizations and arguments of functions are denoted by lower-case letters.

The target is to estimate the failure probability of a truss structure. Failure is defined as an event when the midspan deflection exceeds a given threshold of 0.11 m.

The deflection can be computed using the method of virtual work (unit load method). This method results in a simple expression for the mid-span deflection, $w(\boldsymbol{X})$

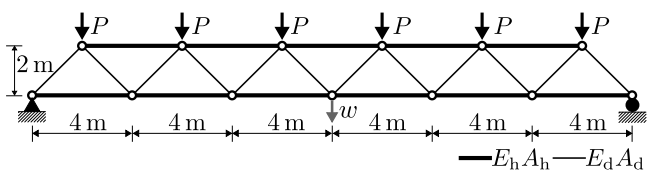

Fig. 10. Truss structure constructed from two types of beams of properties E_{h}, A_{h} (top and bottom horizontal bars) and properties E_{d}, A_{d} (diagonals).

Table 1
Five random variables featured in the truss example.

Variable	Distribution	Mean		CoV
E_{h}, E_{d}	Log-normal	210	GPa	0.10
A_{h}	Log-normal	2000	mm^2	0.10
A_{d}	Log-normal	1000	mm^2	0.10
P	Gumbel-Max	50	kN	0.15

$$w(\boldsymbol{X}) = P\left(\frac{552}{A_{\text{h}}E_{\text{h}}} + \frac{50.9117}{A_{\text{d}}E_{\text{d}}}\right) \quad \equiv \quad P\left(\frac{552}{Æ_{\text{h}}} + \frac{50.9117}{Æ_{\text{d}}}\right) \tag{24}$$

The second expression features only three random variables instead of the five basic variables defined above. The dimensional reduction is made possible by the fact that the couples of variables E and A are always featured together in a product: one can replace both products by defining another variable, $Æ$. The operation is particularly simple here as the products feature two independent variables. The mean value and standard deviation of a product of two independent variables can be easily calculated from the mean values, μ, and standard deviations, σ, of the two variables [22]

$$\mu_{Æ} = \mu_A\,\mu_E, \quad \sigma_{Æ} = \sqrt{\mu_E^2\sigma_A^2 + \mu_A^2\sigma_E^2 + \sigma_E^2\sigma_A^2} \tag{25}$$

The mean value of $Æ_{\text{h}}$ equals 420 MN and the mean value of $Æ_{\text{d}}$ equals 210 MN. The coefficients of variation are identical for both these variables: 0.141 77. The product of two lognormal variables is again a lognormal variable. Using this reduction the problem of a five-dimensional input vector boils down to an entirely equivalent problem that has only three input random variables: the magnitude of forces, P, and two normal cross-sectional stiffnesses, $Æ_{\text{h}}$ and $Æ_{\text{d}}$.

We define the *limit state function* by exploiting the function defined in Eq. (24) as

$$g(\boldsymbol{X}) = 0.11 - w(\boldsymbol{X}) \tag{26}$$

The failure probability is then defined as the probability $p_{\text{f}} = \text{P}[g(\boldsymbol{X}) < 0]$. This translates into the following integral: $p_{\text{f}} = \int_{\mathscr{U}} I[g(\boldsymbol{X}) < 0] f_{\boldsymbol{X}}(\boldsymbol{x})\text{d}\boldsymbol{x}$, where $I[\cdot]$ is the indicator function which equals 1 if $[\cdot]$ is true, and zero otherwise. The indicator function effectively limits the integration domain to combinations of input variables that lead to failure. Each failure event is weighted by the joint probability density function of the input random vector, $f_{\boldsymbol{X}}(\boldsymbol{x})$. Due to the independence of input random variables, the joint density is the product of the marginal probability density functions: $f_{\boldsymbol{X}}(\boldsymbol{x}) = \prod_{v=1}^{N_{\text{var}}} f_v(x_v)$. Using the crude MC method, the failure probability integral is estimated by an average that incorporates the number of failure events, N_{f}, out of all N_{sim} simulations

$$p_{\text{f}} \approx p_{\text{f}}^{\text{MC}} = \frac{1}{N_{\text{sim}}} \sum_{i=1}^{N_{\text{sim}}} I[g(\boldsymbol{x}_i) < 0] = \frac{N_{\text{f}}}{N_{\text{sim}}} \tag{27}$$

The N_{sim} realizations $\boldsymbol{x}_i$ must be sampled proportionally to $f_{\boldsymbol{X}}(\boldsymbol{x})$. The realizations of individual variables can be selected completely independently, taking the marginal densities into account. The individual realizations of sampling probabilities in the unit hypercube are illustrated using blue crosses in Fig. 11 left. These samples are further transformed by inverse distribution functions to the real space where the limit state function is evaluated. Eq. (27) was used to estimate p_{f} using five million MC simulations and the result of $p_{\text{f}}^{\text{MC}} = 0.0404$ was taken as the exact solution.

The difficulty of using MC sampling lies in the fact that the limit state function must be evaluated too many times. When the model is computationally intensive and the failure probability is low, different methods must be used. One possibility is to use the FORM method, which solves the problem in Gaussian space, $\mathscr{G}$. The input random variables and the limit state function can be transformed into $\mathscr{G}$, where one can then identify the so-called *design point*, $\boldsymbol{g}^{\star}$, which is the point on

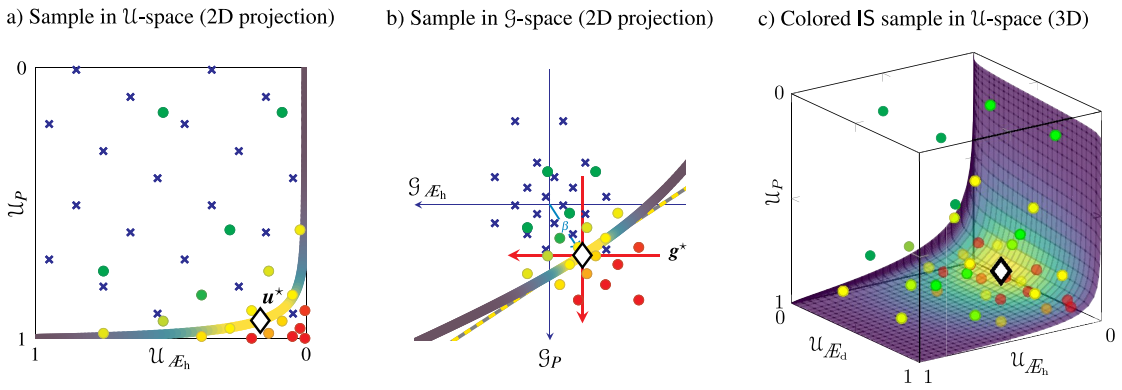

Fig. 11. The process of the transformation of optimized samples (blue crosses) using the sampling density of the IS method to achieve sampling points centered at the design point (highlighted). The color scale of the failure surface corresponds to the Gaussian density in $\mathscr{G}$ space. Depiction of samples: (a) The design point $\boldsymbol{u}^\star$ and the failure surface in $\mathscr{U}$ (2D projection only). (b) The design point $\boldsymbol{g}^\star$ and the failure surface in $\mathscr{G}$ (2D projection only). (c) The design point $\boldsymbol{u}^\star$ and the failure surface in $\mathscr{U}$ in 3D. The red color of the IS points signals failure, while the yellow color signals proximity to the failure surface. (For interpretation of the references to colour in this figure legend, the reader is referred to the web version of this article.)

Table 2
Coordinates of the design point of the truss example in three spaces: $\boldsymbol{x}^\star$, $\boldsymbol{u}^\star$ and $\boldsymbol{g}^\star$. Left: original five-dimensional space. Right: reduced three-dimensional space.

Var.	Physical space		$\mathscr{U}$ space	$\mathscr{G}$ space	α sens.	Var.	Phys. space	$\mathscr{U}$ space	$\mathscr{G}$ space	α sens.
E_h	195.3	GPa	0.2488	− 0.6783	− 0.3811	A_h	363 213 kN	0.1687	− 0.9592	− 0.5389
A_h	1 860	mm^2	0.2488	− 0.6783	− 0.3811					
E_d	206.6	GPa	0.4555	− 0.1117	− 0.0628	A_d	203 336 kN	0.4372	− 0.1580	− 0.0888
A_d	984	mm^2	0.4555	− 0.1117	− 0.0628					
P	62.14	kN	0.9320	1.4910	0.8377	P	62.141 kN	0.9320	1.4910	0.8377

the failure surface $g(\boldsymbol{X}) = 0$ with the highest probability in $\mathscr{G}$ space (it is the nearest point to the origin in $\mathscr{G}$). One can simply perform the linearization of the transformed limit state function in $\boldsymbol{g}^\star$, i.e. the approximation of the actual boundary between the failure set and the safe set by a tangent hyperplane (see the straight line in the 2D projection in Fig. 11b). The estimation of p_f is then made simple via the identification of the distance of $\boldsymbol{g}^\star$ from the origin in $\mathscr{G}$. This distance is denoted β and is called the Hasofer-Lind [24] safety index. Using the $\boldsymbol{g}^\star$ coordinates, $g_v^\star$, in Gaussian space listed in Table 2, the safety index reads $\beta = \sqrt{\sum_{v=1}^{N_{\text{var}}} (g_v^\star)^2} = 1.7799$. With the safety index at hand, the coordinates of $\boldsymbol{g}^\star$ can also be obtained by multiplying β with the directional cosines, i.e. the α sensitivities, see Table 2. By exploiting the rotational symmetry of $\mathscr{G}$, the failure probability can be approximated using the univariate Gaussian cumulative distribution function as $p_f^{\text{FORM}} = \Phi(-\beta) = 0.0375$, a value that is approximately 7% less than the exact solution. The reason for the underestimation is the discrepancy between the approximating hyperplane and the actual failure surface; see the projection in Fig. 11b. The analysis was performed using FReET probabilistic software [52].

In this paper, the coordinates of the most probable failure point are used as the center of the sampling density in Importance Sampling (IS). Instead of sampling the points from the original density, $f_{\boldsymbol{X}}(\boldsymbol{x})$, as performed in Eq. (27), IS selects the samples $\boldsymbol{x}_i$ from the sampling density, $f_{\boldsymbol{X}}^\star(\boldsymbol{x})$, in order to increase the "hit-rate". The sampling density, defined in Gaussian space, is represented by N_{sim} points selected by each of the compared sampling methods. The estimation of failure probability then re-weights the contribution from the "failing" samples using the ratio of the original density to the sampling density

$$p_f \approx \frac{1}{N_{\text{sim}}} \sum_{i=1}^{N_{\text{sim}}} I\left[g(\boldsymbol{x}_i) < 0\right] \frac{f_{\boldsymbol{X}}(\boldsymbol{x}_i)}{f_{\boldsymbol{X}}^\star(\boldsymbol{x}_i)} \tag{28}$$

Since the process is performed in Gaussian space, both densities are computed there simply using the products of univariate Gaussian densities $\mathcal{N}(0, 1)$ and $\mathcal{N}(g_v^\star, 1)$. In other words, the sampling density also has unit dispersion and therefore the difference between the densities lies only in the shifting of the sampling density center from the origin (corresponding to the mean values of the physical variables) to the design point; see the solid red circles Fig. 11 b. The position of the design point in the unit hypercube is visible in Fig. 11, together with DYN samples from the hypercube and those transformed via the shifted sampling density. If the sampling density center is shifted to the design point, we expect roughly half of the points to fall into the failure domain.

Indeed, the *failure surface*, which forms the boundary between the safe and failure regions, contains all points that fulfill the condition $w = 0.11$. Fig. 11 a and b show this boundary in a 2D projection and Fig. 11c shows the failure surface for the reduced 3D problem in the $\mathscr{U}$ space. The color of the surface corresponds to the probability $\prod_{v=1}^{N_{\text{var}}} \phi(g_v)$, where ϕ is the standard univariate Gaussian density function. This density has its peak at the design point, $\boldsymbol{u}^\star$. The figure also shows the importance sample set, colored red in the case of failure, green in the case of a safe structure and yellow when close to the failure surface.

We shall now compare the performance of various sampling schemes in estimating the failure probability using IS around the design point. In particular, the target is defined so as to compare the sample size needed to estimate p_f within ± 10% around the exact value. The probability of failure has been analyzed using Eq. (28) in the full five dimensional space and also in the reduced three-dimensional space, using various sample sizes in both cases (and for each N_{sim} the analysis has been repeated $N_{\text{run}} = 400$ times to obtain variance in the estimations). Only the points falling into the failure region are used. However, distributing them well, i.e. proportionally with respect to the sampling density, may help in improving the accuracy of the estimator in Eq. (28) based on the failing points.

The results are plotted in Fig. 12. By bringing the sampling patterns closer to the region of failure, the samples with optimized uniformity tend to regain their advantage in comparison with estimation using plain MC or LHS samples. Indeed, the graphs show that MC needs the highest number of simulations to produce an estimation lying within the 10% margin of error ($N_{\text{sim}} = 223$ and 580, respectively). Employing

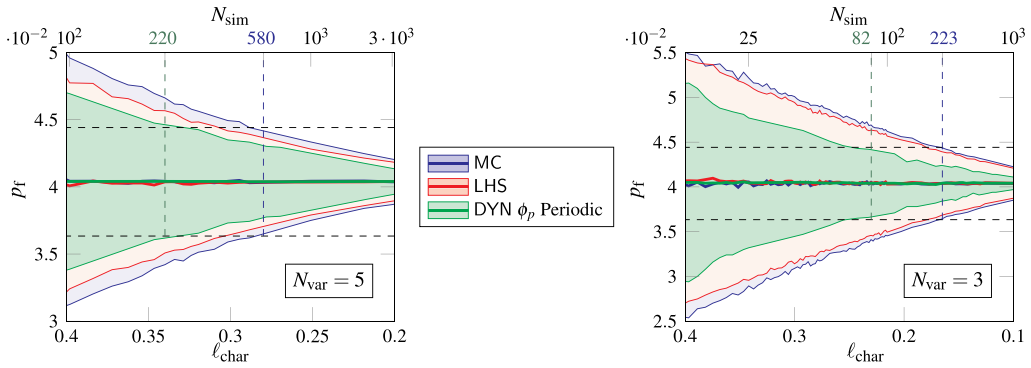

Fig. 12. Convergence of the truss p_f estimation using IS for various sampling methods. Left: the original 5D problem. Right: The reduced 3D problem. Sample sizes needed to estimate p_f within the 10% error margin are highlighted.

LHS stratification along individual dimensions of the Gaussian sampling density helps in reducing in the number of model evaluations, but not much. The proposed DYN samples need approximately one third of that amount of model evaluations to deliver acceptable results (see the marks at $N_{\text{sim}} = 82$ and 220, respectively). We attribute this variance reduction to the higher degree of uniformity achieved for DYN samples.

One can notice that the estimations in five-dimensional space have a greater variance than those for the three dimensional model. This is a property of IS; the difference in variance between the 5D to 3D definition was noticed when any sampling method was employed in IS (MC, LHS and DYN).

The authors also have tested the behavior of the methods for much smaller failure probabilities (10^{-5}). The comparisons look similar and so do the conclusions: employing DYN sampling in IS around the mean values improves accuracy by decreasing the estimator variance.

6. Conclusions

The paper presents a methodology for the construction of uniformly distributed point sets in a hypercubic design domain. The methodology exploits the *analogy* between a distance-based criterion for the point set and a system of repulsive particles. By simulating the dynamical evolution of a damped particle (N-body) system, a near-optimal or even optimal distributions of the particles within the domain is obtained. These final configurations can be readily used as points representing the DYN *design*. By solving the interaction between pairs of particles in a *periodically repeated design domain*, statistically uniform designs are obtained. The distance-based criterion guarantees good sample uniformity, i.e. a uniform spread of points in each single design.

One can also use the family of distance-based criteria for design preparation based on combinatorial optimization techniques [12,82]. However, the proposed dynamical simulation provides a much faster solution to the point arrangements: all the points move in the optimal direction in each time step. Moreover, the derived equations of motion can be efficiently solved by using massive parallelization [41]. The derivation of the equations of motion can be used as a template for similar systems with different potentials.

The authors conject that the decrease in the value of a distance-based criterion that occurs when using a proper metric automatically leads to simultaneous increase of both sample and statistical uniformity of the design. Additionally, it leads to excellent *space-fillingness* and a decrease in *discrepancy*, and naturally guarantees a high degree of *orthogonality*. Projective properties have been found to be excellent, i.e. apart from specific combinations of sample sizes and domain dimensions, the designs are not collapsible. If a design of the LHS type is desired, stratification can be easily achieved by post-processing (latinizing) the DYN sample.

The performance of the designs has been compared to that of other existing designs in various contexts: the estimation of *extremes*, and the *integration* and *statistical estimation* of higher order moments of a function of random variables. Also, an example of increased efficiency when the designs are employed for importance sampling is reported. In all these contexts, the designs perform very well on average: there is no bias and they also exhibit low variance. The designs were found to be superior to Latin Hypercube designs and also more *robust* than several commonly used Quasi Monte Carlo sequences. The designs can be recommended as they provide good support points for initial screening designs or the construction of a surrogate model to replace a computationally intensive model.

The sample size can be easily *extended*, if needed, by preserving the already evaluated points and adding new points in locations with minimal "energy". Evaluation of the local energy provides a hint on positions that can be used to extend the sample size while maintaining uniformity (basically the centers of the largest empty hyperspheres in the periodic design domain). The energy distribution can also be modified to exploit the knowledge about the variation of the function that has been obtained so far, see e.g. [67].

Acknowledgments

The authors acknowledge financial support provided by the Czech Science Foundation under project no. 16-22230S.

Appendix A. The miniMax criterion, its relaxation and analogy to an N-body system

We shall now return to distance-based designs and introduce another class of designs, as well as the possibility of defining the analogy to a system of particles. The Maximin distance criterion (maximization of the minimum distance) and its relaxation into the "repulsive" ϕ_p criterion has been described in Section 2.

Let us now consider designs that attempt to minimize the radius of the largest empty N_{var}-dimensional hypersphere circumscribed to $N_{\text{var}}+1$ design points. By 'empty' it is meant that the hypersphere does not contain any point from $\mathscr{D}$. The maximum radius is the value of the miniMax criterion

$$\phi_{\text{mM}}(\mathscr{D}) = \max_{\boldsymbol{x}\in\mathscr{U}} \min_{\boldsymbol{x}_i} d(\boldsymbol{x}, \boldsymbol{x}_i) \qquad \boldsymbol{x}_i \in \mathscr{D}, \quad \boldsymbol{x} \in \mathscr{U} \tag{A.1}$$

A design that minimizes this measure is said to be a *miniMax* (mM) distance design [29], denoted as $\mathscr{D}_{\text{mM}}$ (note that a more appropriate name would

be miniMaximin). The miniMax design can be illustrated as a solution to the problem of the placement of a store: the maximum distance between any customer (a point $\boldsymbol{x} \in \mathscr{W}$) and their nearest store (a point $\boldsymbol{x}_i \in \mathscr{D}$) should be minimized. One can imagine it as if the center of the largest empty N_{var}-dimensional hypersphere *attracts* the design points (stores), see Fig. 1c.

The evaluation of the maximum radius in Eq. (A.1) can be performed via the construction of a Voronoï diagram in order to localize the center of the largest empty hypersphere. Alternatively, one can approximate it by finding the center within a set of candidate points [42,60]. Regardless of the solution method used, such an evaluation requires heavy computational effort when higher dimensions are involved.

The same type of relaxation that has been applied to the Mm criterion can also be applied to the mM criterion [61,63]. First, the distance from a point $\boldsymbol{x}$ to the nearest design point ($\min_{\boldsymbol{x}_i} d(\boldsymbol{x}, \boldsymbol{x}_i)$) is replaced by a distance from a point $\boldsymbol{x}$ to the whole design consisting of N_{sim} points: $\phi_q = (\sum_i [d(\boldsymbol{x}, \boldsymbol{x}_i)^{-q}])^{-1/q}$ with $q > 0$. This distance measures how well the design $\mathscr{D}$ covers the point $\boldsymbol{x}$. Considering all points in $\mathscr{W}$ leads to an integral that can be approximated by the average of a finite number N_{g} of candidate points (e.g. a fine grid) $\boldsymbol{x}^{(1)}, \ldots, \boldsymbol{x}^{(N_{\text{g}})}$

$$\begin{aligned} \phi_{[p,q]}(\mathscr{D}) &= \left\{ \int_{\mathscr{W}} \left[\sum_{i}^{N_{\text{sim}}} d(\boldsymbol{x}, \boldsymbol{x}_i)^{-q} \right]^{-p/q} \mathrm{d}\boldsymbol{x} \right\}^{1/p} \\ &\approx \left\{ \frac{1}{N_{\text{g}}} \sum_{j=1}^{N_{\text{g}}} \left[\sum_{i}^{N_{\text{sim}}} d(\boldsymbol{x}^{(j)}, \boldsymbol{x}_i)^{-q} \right]^{-p/q} \right\}^{1/p} \end{aligned} \tag{A.2}$$

with $p, q > 0$. We remark that the evaluation of Eq. (A.2) can become rather cumbersome.

Both of the extreme distance-based criteria introduced in [29], namely the Maximin and miniMax criteria, were motivated by the need to select an optimal design for Kriging. We argue that they can also be used to select *statistically uniform* designs, e.g. by employing the periodic metric. This allows them to be used for designs suitable for Monte Carlo integration.

The question still remains as to which class of criterion is more suitable for exploiting the physical analogy proposed in this paper. While with the Maximin criterion one can think of an equivalent to the problem of *packing* N_{sim} hard spheres, the miniMax criterion evokes an attempt to *cover* the design domain $\mathscr{W}$ with N_{sim} balls of minimum radius. Both criteria probably yield a very similar, if not identical, point pattern. There are known relationships existing between the Maximin and miniMax criteria, and also bounds on their optimal values, as explained in [60].

We shall now advocate our preference for the *relaxed* versions of potentials over the extremal potentials (Mm and mM) originally introduced in [29]. In the case of the raw miniMax and Maximin criteria, repulsive or attractive forces are supposed to act upon the pair of closest points or $(N_{\text{var}} + 1)$ most distant points, respectively. In this case the definition of the energy potential is not known in advance and changes abruptly during the simulation with a dependence on mutual distances. Moreover, due to the absolutely uncompromising goal of the maximization or minimization of selected distances, the forces applied to the bodies tend to infinity. This renders the raw Maximin or miniMax criteria quite unsuitable as templates for the potential energy of a dynamical system. For such "binary" energy potentials, a more convenient type of simulation can be found in a quasi-dynamic *marching* simulation that discretizes the translation of bodies rather than time. In such a simulation, the momenta and velocities of bodies shall be omitted in order to obey the "on-off" nature of these criteria.

On the other hand, the relaxed variants, i.e. the relaxed generalized miniMax and especially the ϕ_p criterion, do exhibit desirable properties in this regard. These criteria consider (i) all bodies to be affected by repelling/attracting forces and more importantly (although both are unrestricted power laws) (ii) propose better-posed formulations of potential energy than their raw counterparts.

While the ϕ_p criterion has an analogy to *mutually repelling bodies*, the relaxed mM criterion is analogical to *bodies attracted* by the points in the design domain, see Fig. 1. The major advantage of the ϕ_p energy potential, however, lies in the origin of the repulsive forces acting upon a finite number of bodies. Unlike the attracting forces of the relaxed miniMax potential that are generated by the continuous volume of the entire design domain, the ϕ_p-forces that mutually repel pairs of particles are generated by the "charged" particles themselves. Due to this, the actual formulations of ϕ_p and the relaxed mM energy potentials differ significantly. A ϕ_p-repulsive force acting upon a particle is the sum of $(N_{\text{sim}} - 1)$ discrete contributions from all other repelling bodies. The mM-attractive forces, quite inconveniently, are integrated over the continuous volume of the design domain itself. Considering the above, the ϕ_p criterion does seem to be the most convenient option. It produces an energy potential that inherently provides a finite number $(N_{\text{sim}} \cdot N_{\text{var}})$ of equations of motion, each of which contains a finite number of $N_{\text{sim}} - 1$ known contributions. That is why that criterion was selected for the derivation in the present paper.

Appendix B. Error $\epsilon(E)$ for regular orthogonal and regular simplex grids

We now derive the average error in estimating the peak of the testing function in Eq. (18) in an N_{var} dimensional periodic domain when the design used for estimation forms two simple regular grids: a regular orthogonal grid and a regular simplex grid. Let us remember that the length scale parameter in the testing function has been selected so that it depends on the average density of points (in point processes the *intensity*) via ℓ_{char}.

In order to calculate the mean error and also its standard deviation when sliding the center of the testing function over the regular point pattern, one can reduce the problem of calculating these characteristics over a domain that belongs to one individual sampling point. A region belonging to that point must be taken so that the points are closer to this point than to any other point in the pattern.

B1. Regular orthogonal grid

In the case of arrangement into a regular orthogonal grid, the region $\mathscr{K}$ nearest to a single point is simply a hypercube of edge length $a = \ell_{\text{char}}$ (the point spacing along each dimension is ℓ_{char}), see Fig. B.13a. The mean value of error $\epsilon(E)$, is denoted as $\mu_{\mathscr{K}}$, and the standard deviation is denoted $\sigma_{\mathscr{K}}$. Their computation involves the integration of f raised to integer powers and weighted by a uniform density, and the integration domain is $\mathscr{K}$. With no loss in generality, we consider the characteristic length $a = \ell_{\text{char}} = 1$. Therefore, the volume of the integration region is: $V_{\mathscr{K}} = V_{\mathscr{F}} = 1$. Two integrals are needed

$$m_1^{(\mathscr{K})} = \int_{-1/2}^{1/2} \cdot \int_{-1/2}^{1/2} f(\boldsymbol{x})\, \mathrm{d}\boldsymbol{x} = \left[\sqrt{\pi} \cdot \mathrm{erf}\left(\frac{1}{2}\right) \right]^{N_{\text{var}}} \tag{B.1}$$

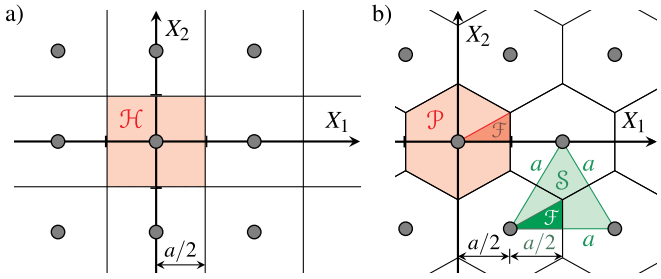

Fig. B.13. Two-dimensional illustration of two regular point arrangements and the corresponding integration domains. (a) Regular orthogonal grid. (b) Regular triangular grid.

Table B.3
Errors $\epsilon(E)$ for two models of regular grids. Standard deviations must be multiplied by 10^{-2}.

N_{var}	Orthogonal grid		Simplex grid	
	$\mu_{\mathscr{H}}$	$\sigma_{\mathscr{H}}$	$\mu_{\mathscr{P}}$	$\sigma_{\mathscr{P}}$
1	0.077 38	6.710 98	0.077 38	6.710 98
2	0.148 88	8.767 39	0.144 41	8.011 58
3	0.214 78	9.919 41	0.197 94	8.212 09
4	0.275 59	10.58 10	0.240 78	8.000 34
5	0.331 69	10.92 83	0.275 61	7.634 71

$$m_2^{(\mathscr{H})} = \int_{\mathscr{H}} f^2(\boldsymbol{x})\,\mathrm{d}\boldsymbol{x} = \left[\sqrt{\frac{\pi}{2}}\cdot\mathrm{erf}\left(\frac{\sqrt{2}}{2}\right)\right]^{N_{\text{var}}} \tag{B.2}$$

With these solutions at hand, the mean value and variance of the error $\epsilon(E)$ read

$$\mu_{\mathscr{H}} = 1 - \frac{m_1}{V_{\mathscr{F}}} \qquad \sigma^2_{\mathscr{H}} = \frac{m_2 V_{\mathscr{F}} - m_1^2}{V^2_{\mathscr{F}}} \tag{B.3}$$

The umerical solutions are summarized in Table B.3. The mean values are marked by an empty square and the $\mu_{\mathscr{H}} \pm \sigma_{\mathscr{H}}$ are marked by the error bars around the squares in Fig. 8. It can be seen that this arrangement of points is not the most efficient one and that the DYN designs are able to identify the extremes of $f()$ more accurately; see the green lines.

B2. Regular simplex grid

We consider one of the best possible uniform arrangements of points with a given density to be a kind of "hypertriangular grid": the design points form regular *simplexes*. The regions around each point (centroids of the simplexes) are regular polyhedra, $\mathscr{P}$, sketched as 2D honeycombs in Fig. B.13b. The generalization of such a grid to a higher dimension is trivial. Unfortunately, this grid is not periodic.

Due to the regularity of the domain $\mathscr{P}$, the integration can be limited to a typical *fragment* $\mathscr{F}$, see Fig. B.13b. This fragment is repeated $N_{\text{var}}![(N_{\text{var}}+1)!]$ times within $\mathscr{P}$.

The volume of the fragment can easily be calculated with the help of a *regular simplex*, herein denoted as region $\mathscr{S}$. This regular simplex is obtained by enclosing the nearest $N_{\text{var}}+1$ points with hyperplanes. The regular simplex takes the form of a triangle, tetrahedron, 5-cell, etc. This simplex has also the region $\mathscr{F}$ as its fragment, now repeated $(N_{\text{var}}+1)!$ times inside of it. By denoting the side of the simplex by a, which is the smallest distance between points, the volumes of the regular simplex, the polyhedron around a point and its typical fragment for integration, read

$$V_{\mathscr{S}}(a, N_{\text{var}}) = a^{N_{\text{var}}}\frac{1}{N_{\text{var}}!}\sqrt{\frac{N_{\text{var}}+1}{2^{N_{\text{var}}}}} \tag{B.4}$$

$$V_{\mathscr{P}} = N_{\text{var}}!V_{\mathscr{S}} \tag{B.5}$$

$$V_{\mathscr{F}} = \frac{V_{\mathscr{S}}}{(N_{\text{var}}+1)!} \tag{B.6}$$

Once the volume of the polyhedron belonging to a point is known, one can calculate the characteristic (scaling) length for Eq. (18). It is the N_{var}th root of the volume associated with a point

$$\ell_{\text{char}} = \sqrt[N_{\text{var}}]{V_{\mathscr{P}}} = a\sqrt{\frac{(N_{\text{var}}+1)^{1/N_{\text{var}}}}{2}} \tag{B.7}$$

All that remains is to perform integrals analogical to Eq. (B.1), weighted uniformly (divided by the fragment volume). The first two moments of the function read:

$$m_1^{(\mathscr{P})} = \int_{x_1=0}^{\frac{a}{2}}\int_{x_2=0}^{\frac{x_1}{\sqrt{3}}}\int_{x_3=0}^{\frac{x_2}{\sqrt{2}}}\cdots\int_{x_\nu=0}^{k_\nu x_{\nu-1}} f(\boldsymbol{x})\prod_{\nu=1}^{N_{\text{var}}}\mathrm{d}x_\nu \tag{B.8}$$

$$m_2^{(\mathscr{P})} = \int_{\mathscr{F}} f^2(\boldsymbol{x})\,\mathrm{d}\boldsymbol{x} \tag{B.9}$$

in both of which the domain of integration, $\mathscr{F}$, is identical: the first bound for x_1 is a constant, $a/2$, which is the middle distance to the nearest point, see Fig. B.13a. All the remaining upper bounds are linear functions enclosing the fragment: $k_v\, x_{v-1} = \sqrt{(v-1)/(v+1)}\, x_{v-1}$. The integrals involve error functions and are not obtainable in analytical form. Again, the first two raw moments can be used in Eq. (B.3), together with $V_{\mathscr{F}}$, to obtain the mean value, $\mu_{\mathscr{P}}$, and standard deviation, $\sigma_{\mathscr{P}}$, of the errors; see Table B.3.

We remark that these solutions cannot be obtained by any periodic design, i.e. the error of real designs must always be greater. Lattices obtainable in practice usually resemble the regular simplex grid, but these are always somehow "stretched", which results in greater errors. Indeed, Fig. 8 shows that DYN solutions, which often form perfect lattices, have slightly greater errors than the theoretically derived limits here, which are marked by empty diamonds with error-bars corresponding to $\mu_{\mathscr{P}} \pm \sigma_{\mathscr{P}}$.

References

[1] Athanassoula E, Fady E, Lambert J, Bosma A. Optimal softening for force calculations in collisionless n-body simulations. Monthly Notices R Astron Soc 2000;314(3):475–88. https://doi.org/10.1086/172641.

[2] Audze P, Eglājs V. New approach for planning out of experiments. Probl Dyn Streng 1977;35:104–7. (in Russian)

[3] Bates S, Sienz J, Langley D. Formulation of the Audze–Eglais uniform latin hypercube design of experiments. Adv Eng Softw 2003;34(8):493–506. https://doi.org/10.1016/S0965-9978(03)00042-5.

[4] Blatman G, Sudret B. An adaptive algorithm to build up sparse polynomial chaos expansions for stochastic finite element analysis. Probab Eng Mech 2010;25(2):183–97. https://doi.org/10.1016/j.probengmech.2009.10.003.

[5] Burnaev E, Panin I, Sudret B. Efficient design of experiments for sensitivity analysis based on polynomial chaos expansions. Ann Math Artif Intell 2017;81(1):187–207. https://doi.org/10.1007/s10472-017-9542-1.

[6] Cioppa TM, Lucas TW. Efficient nearly orthogonal and space-filling latin hypercubes. Technometrics 2007;49(1):45–55. https://doi.org/10.1198/004017006000000453.

[7] Conover W.J.. On a better method for selecting input variables; 1975. Unpublished Los Alamos National Laboratories manuscript, reproduced as Appendix A of "Latin Hypercube Sampling and the Propagation of Uncertainty in Analyses of Complex Systems" by J.C. Helton and F.J. Davis, Sandia National Laboratories report SAND2001-0417.

[8] Couckuyt I, Forrester A, Gorissen D, Turck FD, Dhaene T. Blind kriging: implementation and performance analysis. Adv Eng Softw 2012;49:1–13. https://doi.org/10.1016/j.advengsoft.2012.03.002.

[9] Cranley R, Patterson TNL. Randomization of number theoretic methods for multiple integration. SIAM J Numer Anal 1976;13(6):904–14. https://doi.org/10.1137/0713071.

[10] Dean A, Morris M, Stufken J, Bingham D. Handbook of design and analysis of experiments. Chapman & Hall/CRC Handbooks of Modern Statistical Methods CRC Press; 2015. ISBN 978-1-4665-0434-9

[11] Deutsch JL, Deutsch CV. Latin hypercube sampling with multidimensional uniformity. J Stat Plann Infer 2012;142(3):763–72. https://doi.org/10.1016/j.jspi.2011.09.016.

[12] Eliáš J, Vořechovský M. Modification of the Audze–Eglājs criterion to achieve a uniform distribution of sampling points. Adv Eng Softw 2016;100:82–96. https://doi.org/10.1016/j.advengsoft.2016.07.004.

[13] Erkut E. The discrete p-dispersion problem. Eur J Operat Res 1990;46(1):48–60. https://doi.org/10.1016/0377-2217(90)90297-O.

[14] Fang K-T, Wang Y. Number-theoretic methods in statistics. 1st ed. London ; New York: Chapman and Hall/CRC; 1993. ISBN 9780412465208

[15] Fang K-T, Wang Y, Bentler PM. Some applications of number-theoretic methods in statistics. Stat Sci 1994;9(3):416–28. https://doi.org/10.1214/ss/1177010392.

[16] Fang K-T, Lin DKJ, Winker P, Zhang Y. Uniform design: theory and application. Technometrics 2000;42(3):237–48. https://doi.org/10.2307/1271079.

[17] Faure H. Discrépances de suites associées à un système de numération (en dimension un) [discrepancy of sequences associated with a number system (in dimension one)]. Bulletin de la Société Mathématique de France 1981;109.

[18] Fuerle F, Sienz J. Formulation of the Audze–Eglais uniform latin hypercube design of experiments for constrained design spaces. Adv Eng Softw 2011;42(9):680–9. https://doi.org/10.1016/j.advengsoft.2011.05.004.

[19] Ghiocel DM, Ghanem RG. Stochastic finite-element analysis of seismic soil-structure interaction. J Eng Mech 2002;128(1):66–77. https://doi.org/10.1061/(ASCE)0733-9399(2002)128:1(66).

[20] Giovanis DG, Papadopoulos V. Spectral representation-based neural network assisted stochastic structural mechanics. Eng Struct 2015;84:382–94. https://doi.org/10.1016/j.engstruct.2014.11.044.

[21] Goel T, Haftka RT, Shyy W, Watson LT. Pitfalls of using a single criterion for selecting experimental designs. Int J Numer Methods Eng 2008;75(2):127–55. https://doi.org/10.1002/nme.2242.

[22] Goodman LA. On the exact variance of products. J Am Stat Assoc 1960;55(292):708–13. https://doi.org/10.1080/01621459.1960.10483369.

[23] Halton J. On the efficiency of certain quasi-random sequences of points in evaluating multi-dimensional integrals. Numer Math 1960;2(1):84–90. https://doi.org/10.1007/BF01386213.

[24] Hasofer AM, Lind NC. An exact and invariant first order reliability format. J Eng Mech 1974;100:111–21.

[25] Hickernell FJ. A generalized discrepancy and quadrature error bound. Math Comput 1998;67(221):299–322. https://doi.org/10.1090/S0025-5718-98-00894-1.

[26] Husslage BG, Rennen G, van Dam ER, den Hertog D. Space-filling latin hypercube designs for computer experiments. Optim Eng 2011;12(4):611–30. https://doi.org/10.1007/s11081-010-9129-8.

[27] Iman RC, Conover WJ. A distribution free approach to inducing rank correlation among input variables. Commun Stat 1982;B11:311–34. https://doi.org/10.1080/03610918208812265.

[28] Jin R, Chen W, Sudjianto A. An efficient algorithm for constructing optimal design of computer experiments. J Stat Plann Infer 2005;134(1):268–87. https://doi.org/10.1016/j.jspi.2004.02.014.

[29] Johnson M, Moore L, Ylvisaker D. Minimax and maximin distance designs. J Stat Plann Infer 1990;2(26):131–48. https://doi.org/10.1016/0378-3758(90)90122-B.

[30] Joseph VR. Space-filling designs for computer experiments: a review. Qual Eng 2016;28(1):28–35. https://doi.org/10.1080/08982112.2015.1100447.

[31] Joseph VR, Hung Y. Orthogonal-maximin latin hypercube designs. Stat Sin 2008;18(1):171–86. https://doi.org/10.2307/24308251.

[32] Koksma JF. Een algemeene stelling uit de theorie der gelijkmatige verdeeling modulo 1. Math B 1942/1943;11:7–11.

[33] Kroetz HM, Tessari RK, Beck AT. Performance of global metamodeling techniques in solution of structural reliability problems. Adv Eng Softw 2017;114:394–404. https://doi.org/10.1016/j.advengsoft.2017.08.001.

[34] L'Ecuyer P, Lemieux C. Modeling Uncertainty: An Examination of Stochastic Theory, Methods, and Applications. International Series in Operations Research & Management Science; chapter Recent Advances in Randomized Quasi-Monte Carlo Methods 46. Springer, New York, NY; 2002. p. 419–74. https://doi.org/10.1007/b106473. ISBN 978-0-7923-7463-3,978-0-306-48102-4, Part V

[35] Lee SH, Kwak BM. Response surface augmented moment method for efficient reliability analysis. Struct Safety 2006;28(3):261–72. https://doi.org/10.1016/j.strusafe.2005.08.003.

[36] Lemieux C, Owen AB. Quasi-regression and the relative importance of the Anova components of a function. In: Fang K-T, Niederreiter H, Hickernell FJ, editors. Monte Carlo and Quasi-Monte Carlo Methods 2000 Berlin, Heidelberg: Springer Berlin Heidelberg; 2002. p. 331–44. https://doi.org/10.1007/978-3-642-56046-0_22. ISBN 978-3-642-56046-0

[37] Li P, Li H, Huang Y, Wang K, Xia N. Quasi-sparse response surface constructing accurately and robustly for efficient simulation based optimization. Adv Eng Softw 2017;114:325–36. https://doi.org/10.1016/j.advengsoft.2017.07.014.

[38] Liefvendahl M, Stocki R. A study on algorithms for optimization of latin hypercubes. J Stat Plann Inf 2006;136(9):3231–47. https://doi.org/10.1016/j.jspi.2005.01.007.

[39] Lillie HR, Ritland HN. Fine annealing of optical glass. J Am Ceram Soc 1954;37(10):466–73. https://doi.org/10.1111/j.1151-2916.1954.tb13978.x.

[40] Mašek J, Vořechovský M. On the influence of the interaction laws of a dynamical particle system for sample optimization. Trans VŠB -Tech Uni Ost 2017;17(1):137–46. https://doi.org/10.1515/tvsb-2017-0016.

[41] Mašek J, Vořechovský M. Parallel implementation of hyper-dimensional dynamical particle system on CUDA. Adv Eng Softw 2018;125:178–87. https://doi.org/10.1016/j.advengsoft.2018.03.009.

[42] Mašek J, Vořechovský M. Approximation of Voronoï cell attributes using parallel solution. Adv Eng Softw 2019;132:7–17. https://doi.org/10.1016/j.advengsoft.2019.03.012.

[43] McKay MD, Conover WJ, Beckman RJ. A comparison of three methods for selecting values of input variables in the analysis of output from a computer code. Technometrics 1979;21:239–45. https://doi.org/10.1080/00401706.1979.10489755.

[44] Morris MD, Mitchell TJ. Exploratory designs for computational experiments. J Stat Plann Inf 1995;43(3):381–402. https://doi.org/10.1016/0378-3758(94)00035-T.

[45] Niederreiter H. Studies in Pure mathematics: to the memory of Paul Turán, chapter A quasi-Monte Carlo method for the approximate computation of the extreme values of a function. Basel: Birkhäuser Basel; 1983. p. 523–9. https://doi.org/10.1007/978-3-0348-5438-2. ISBN 978-3-0348-5438-2

[46] Niederreiter H. Point sets and sequences with small discrepancy. Monatshefte für Mathematik 1987;104(4):273–337. https://doi.org/10.1007/BF01294651.

[47] Niederreiter H. Low-discrepancy and low-dispersion sequences. J Number Theory 1988;30(1):51–70. https://doi.org/10.1016/0022-314X(88)90025-X.

[48] Niederreiter H. Random number generation and quasi-monte carlo methods. CBMS-NSF Regional Conference Series in Applied Mathematics Philadelphia,

Pennsylvania: Society for industrial and applied mathematics; 1992. https://doi.org/10.1137/1.9781611970081. ISBN 978-0-898712-957
[49] Niederreiter H. Random number generation and quasi-monte carlo methods. Soc Ind Appl Math (SIAM); 1992. https://doi.org/10.1137/1.9781611970081. ISBN 978-0-898712-95-7
[50] Novák D, Teplý B, Keršner Z. The role of latin hypercube sampling method in reliability engineering. In: Shiraishi N, Shinozuka M, Wen YK, editors. Proceedings of the 7th international conference on structural safety and reliability ICoSSaR '97,. 2. Kyoto, Japan: Rotterdam Balkema; 1998. p. 403–9.
[51] Novák D, Lehký D. ANN Inverse analysis based on stochastic small-sample training set simulation. Eng Appl Artif Intell 2006;19(7):731–40. https://doi.org/10.1016/j.engappai.2006.05.003. Special issue on Engineering Applications of Neural Networks – Novel Applications of Neural Networks in Engineering
[52] Novák D, Vořechovský M, Teplý B. FReEt: software for the statistical and reliability analysis of engineering problems and FReET-D: degradation module. Adv Eng Softw 2014;72:179–92. https://doi.org/10.1016/j.advengsoft.2013.06.011.
[53] Olsson A, Sandberg G, Dahlblom O. On latin hypercube sampling for structural reliability analysis. Struct Safety 2003;25(1):47–68. https://doi.org/10.1016/S0167-4730(02)00039-5.
[54] Owen AB. A central limit theorem for latin hypercube sampling. J R Stat Soc Ser B (Methodol) 1992;54(2):541–51. https://doi.org/10.2307/2346140.
[55] Owen AB. Controlling correlations in latin hypercube samples. J Am Stat Assoc (Theory Methods) 1994;89(428):1517–22. https://doi.org/10.2307/2291014.
[56] Owen AB. Monte carlo and quasi-monte carlo methods in scientific computing. Lecture Notes in Statistics; chapter Randomly permuted (*t; m; s*)-nets and (*t; s*)-sequences 106. Springer-Verlag New York; 1995. p. 299–317. ISBN 978-0-387-94577-4,978-1-4612-2552-2 Proceedings of a conference at the University of Nevada, Las Vegas, Nevada, USA, June 23–25, 1994
[57] Owen AB. Monte-Carlo and Quasi-Monte Carlo Methods 1998, chapter Monte Carlo quasi-Monte Carlo and randomized quasi-Monte Carlo. Lecture Notes in Statistics Springer-Verlag Berlin Heidelberg; 1999. p. 86–97. ISBN 978-3-540-66176-4 Proceedings of a Conference held at the Claremont Graduate University, Claremont, California, USA, June 22–26, 1998
[58] Park J-S. Optimal latin-hypercube designs for computer experiments. J Stat Plann Inf 1994;39(1):95–111. https://doi.org/10.1016/0378-3758(94)90115-5.
[59] Pholdee N, Bureerat S. An efficient optimum latin hypercube sampling technique based on sequencing optimisation using simulated annealing. Int J Syst Sci 2015;46(10):1780–9. https://doi.org/10.1080/00207721.2013.835003.
[60] Pronzato L. Minimax and maximin space-filling designs: some properties and methods for construction. J de la Société Française de Statistique 2017;158(1):7–36.
[61] Pronzato L, Müller WG. Design of computer experiments: space filling and beyond. Stat Comput 2012;22(3):681–701. https://doi.org/10.1007/s11222-011-9242-3.
[62] Ronco CCD, Ponza R, Benini E. Aerodynamic shape optimization of aircraft components using an advanced multi-objective evolutionary approach. Comput Methods Appl Mech Eng 2015;285(0):255–90. https://doi.org/10.1016/j.cma.2014.10.024.
[63] Royle JA, Nychka D. An algorithm for the construction of spatial coverage designs with implementation in SPLUS. Comput Geosci Arch 1998;24(5):479–88. https://doi.org/10.1016/S0098-3004(98)00020-X.
[64] Sallaberry C, Helton J, Hora S. Extension of latin hypercube samples with correlated variables. Reliab Eng Syst Saf 2008;93(7):1047–59. https://doi.org/10.1016/j.ress.2007.04.005.
[65] Santner TJ, Williams BJ, Notz WI. The design and analysis of computer experiments. Springer Series in Statistics Springer-Verlag New York; 2003. https://doi.org/10.1007/978-1-4757-3799-8. ISBN 978-0-387-95420-2
[66] Schonlau M, Welch WJ. Screening, chapter screening the input variables to a computer model via analysis of variance and visualization. Springer, New York, NY; 2006. p. 308–27. https://doi.org/10.1007/0-387-28014-6. ISBN 978-0-387-28013-4
[67] Shields MD. Adaptive monte carlo analysis for strongly nonlinear stochastic systems. Reliab Eng Syst Saf 2018;175:207–24. https://doi.org/10.1016/j.ress.2018.03.018.
[68] Shields MD, Zhang J. The generalization of latin hypercube sampling. Reliab Eng Syst Saf 2016;148:96–108. https://doi.org/10.1016/j.ress.2015.12.002.
[69] Shields MD, Teferra K, Hapij A, Daddazio RP. Refined stratified sampling for efficient monte carlo based uncertainty quantification. Reliab Eng Syst Saf 2015;142:310–25. https://doi.org/10.1016/j.ress.2015.05.023.
[70] Sobol' IM. On the distribution of points in a cube and the approximate evaluation of integrals. USSR Comput Math Math Phys 1967;7(4):784–802. https://doi.org/10.1016/0041-5553(67)90144-9.
[71] Sobol' IM. Uniformly distributed sequences with an additional uniform property. USSR Comput Math Math Phys 1976;16(5):236–42. https://doi.org/10.1016/0041-5553(76)90154-3. Short communication
[72] Stein M. Large sample properties of simulations using latin hypercube sampling. Technometrics 1987;29(2):143–51. https://doi.org/10.1080/00401706.1987.10488205.
[73] Steiner M, Bourinet J-M, Lahmer T. An adaptive sampling method for global sensitivity analysis based on least-squares support vector regression. Reliab Eng Syst Saf 2019;183:323–40. https://doi.org/10.1016/j.ress.2018.11.015.
[74] Talke IS, Borkowski JJ. Generation of space-filling uniform designs in unit hypercubes. J Stat Plann Inf 2012;142(12):3189–200. https://doi.org/10.1016/j.jspi.2012.06.013.
[75] Tang B. Orthogonal array-based latin hypercubes. J Am Stat Assoc 1993;88(424):1392–7. https://doi.org/10.1080/01621459.1993.10476423.
[76] Tezuka S. Uniform Random Numbers: Theory and Practice. The springer international series in engineering and computer science 315. Springer, Boston, MA; 1995. https://doi.org/10.1007/978-1-4615-2317-8. ISBN 978-1-4613-5980-7,978-1-4615-2317-8
[77] Tong C. Refinement strategies for stratified sampling methods. Reliab Eng Syst Saf 2006;91(10–11):1257–65. https://doi.org/10.1016/j.ress.2005.11.027.
[78] Viana FAC, Venter G, Balabanov V. An algorithm for fast optimal latin hypercube design of experiments. Int J Numer Methods Eng 2010;82(2):135–56. https://doi.org/10.1002/nme.2750.
[79] Vořechovský M. Optimal singular correlation matrices estimated when sample size is less than the number of random variables. Probab Eng Mech 2012;30:104–16. https://doi.org/10.1016/j.probengmech.2012.06.003.
[80] Vořechovský M. Correlation control in small sample monte carlo type simulations II: analysis of estimation formulas, random correlation and perfect uncorrelatedness. Probab Eng Mech 2012;29:105–20. https://doi.org/10.1016/j.probengmech.2011.09.004.
[81] Vořechovský M. Hierarchical refinement of latin hypercube samples. Comput Aided Civil Infrast Eng 2015;30(5):1–18. https://doi.org/10.1111/mice.12088.
[82] Vořechovský M, Novák D. Correlation control in small sample monte carlo type simulations i: a simulated annealing approach. Probab Eng Mech 2009;24(3):452–62. https://doi.org/10.1016/j.probengmech.2009.01.004.
[83] Vořechovský M, Eliáš J. Modification of the maximin and ϕ_p (phi) criteria to achieve statistically uniform distribution of sampling points. Technometrics 2019. https://doi.org/10.1080/00401706.2019.1639550. in press
[84] Weyl H. Über die gleichverteilung von zahlen mod. Eins [on the distribution of numbers modulo one]. Math Ann 1916;77(3):313–52. https://doi.org/10.1007/BF01475864.